Department of Earth and Planetary Sciences
Massachusetts Institute of Technology
Cambridge, Massachusetts 02139

RESEARCH IN SEISMOLOGY

Semi-Annual Technical Report No. 6

Period Covered: 1 January 1978 - 30 June 1978

ARPA Order No. 1827

Program Code No. 5F10

Name of Contractor - M.I.T.

Effective Date of Contract - 1 June 1975

Contract Expiration Date - 30 September 1979

Amount of Contract - $615,000

Contract No. - F44620-75-C-0064

Principal Investigators - M. Nafi Toksöz, 617/253-6382
Keiiti Aki, 617/253-6397
Sean C. Solomon, 617/253-3786

Program Manager - William J. Best, 202/694-5454

Short Title of Work - Research in Seismology

Sponsored by

Advanced Research Projects Agency

ARPA Order No. 1827

1. SUMMARY

The research completed under the contract F44620-75-C-0064 "Research in Seismology" during the period 1 January 1978 - 30 June 1978 falls within the two broad topics of (1) Seismic source mechanisms and (2) Seismic wave propagation. The specific research tasks within each category have broad applicability to the problem of discrimination of earthquakes from underground nuclear explosions, with particular emphasis on the Asian continent.

Source mechanism investigations included continued detailed studies of earthquakes in eastern Turkey from the standpoint of field and teleseismic observations and of precursory phenomena (Nabelek and Toksöz, 1978a,b) and a new look at the earthquake mechanism and stress drop from the standpoint of a model fault with barriers (Aki, 1978). Wave propagation work included studies of attenuation mechanisms in rock (Johnston and Cheng, 1978), attenuation and shear wave delay beneath the Mid-Atlantic Ridge (Muller et al., 1978), and the further application of a technique for simultaneous inversion of surface wave attenuation and phase velocity information to data from several continental and oceanic paths (Lee and Solomon, 1979).

Details of these studies are given in the preprint and abstracts in the following sections. A cumulative list of publications completed under the contract is also included.

2. SEISMIC SOURCE MECHANISMS

SOURCE PROPERTIES OF THE 1976 EARTHQUAKE IN E. TURKEY

NABELEK, J.L. AND TOKSÖZ, M.N., Department of Earth and Planetary Sciences, Massachusetts Institute of Technology, Cambridge, MA 02139

The Eastern Turkey earthquake on 24 November 1976 (M_S = 7.3) provided good data for testing the validity of source models by comparing geological observations at the source and seismic observations at teleseismic distances. A steeply dipping fault was traced for 55 km with an average strike of N70°W. The motion was essentially right-handed strike slip with an average displacement of 2.5-3 m. Water level marks along the shore of Lake Van provided an estimate of the regional tilt.

The fault plane solution obtained from P-wave polarities and the surface wave radiation pattern is well constrained with a strike: N73°W, dip: 78°S and slip angle: 4°. The width of the fault was about 25 km, based upon static dislocation theory and shape of the surface wave spectra. Seismic moment calculated on the basis of static and dynamic source models was 1.4×10^{27} and 0.7×10^{27} dyne-cm respectively. Slight disagreement between two values may be due to frequency dependence of the moment, aseismic creep or aftershocks. The stress drop was 35 bars.

Presented at: Seismological Society of America Annual Meeting
April, 1978
Sparks, Nevada

Eastern Turkey Earthquake of 24 November 1976 - A Comparative Study

J. Nabelek and M.N. Toksöz

The 24 November 1976 earthquake in the Van Province of eastern Turkey was a large (M_S = 7.3) strike-slip event. A comparison of this earthquake with the 1976 Guatemala event can provide a better understanding of the dynamics of strike-slip faulting. Geological observations in the source area of the Turkish earthquake are well documented. Surface expressions of the fault could be traced clearly for 55 km. Average displacements along the dislocation vectors were 3 - 2.5 m. The dip was almost vertical. Water level marks along the shore of Lake Van provided an estimate of the regional tilt. A few physical precursory phenomena were also observed. Seismic moment and source mechanism were determined both from field observations in the source region and seismic records at teleseismic distances. The agreement is excellent for the orientation of the fault. However, seismic moment determined from surface wave data (7×10^{26} dyne-cm) is about 2 times smaller than the static moment estimate. The reverse was observed for the Guatemalan earthquake. The geometry of the two events is different. The Turkish fault zone is relatively short and wide (55 km and 25 km respectively), with large displacements (2.5 m). Faulting in the Guatemalan event was about 250 km long with average surface displacements of about 1.0 m. Differences between the source parameters of the two earthquakes may be due to differences in stress regime, age of the fault, or thickness of the brittle layer.

Presented at: International Symposium on the February 4, 1976 Guatemalan Earthquake and the Reconstruction Process
May, 1978
Guatemala City

STRESS DROP AND ENERGY RELEASE IN AN EARTHQUAKE ESTIMATED BY THE USE OF THE BARRIER MODEL

Keiiti Aki, (Dept. of Earth & Planetary Sciences, Mass. Inst. of Techn., Cambridge, MA 02139)

So far, the stress drop in an earthquake has been estimated by assuming a fault plane without any obstacles, mismatches, or barriers. On the other hand, observations of slip along a fault at the surface, observations of short-period seismic waves near a fault and at far-field, and scaling relations for small earthquakes in various seismic regions suggest that the fault plane with distributed barriers which remain unbroken after rupture propagation may be more realistic than a smoothly ruptured fault plane. By numerical experiments on spontaneous shear-crack propagation, Das and Aki (1977) demonstrated the mechanical feasibility of such a model of a fault plane with distributed unbroken barriers. Application of the barrier model to actual data leads to a disturbing conclusion that the stress drop in major earthquakes might have been underestimated by an order of magnitude. The model also requires the apparent stress to be an order of magnitude greater than earlier estimates. Then, we face another disturbing result in that the Gutenberg-Richter's magnitude-energy formula may be underestimating seismic energy by an order of magnitude. The estimated high ambient tectonic stress is more consistent with the frictional strength of rocks measured in laboratories. Such a high stress, however, cannot be maintained by plate boundary forces such as slab-pull and ridge-push, but requires a basal-shear due to convection in the upper mantle as discussed by Hanks (1977).

Presented at: American Geophysical Union
Spring Annual Meeting
April, 1978
Miami Beach, Florida

3. SEISMIC WAVE PROPAGATION

THE ROLE OF FLUID FLOW IN ATTENUATION

David H. Johnston
C.H. Cheng (both at: Dept. of Earth and Planetary Sciences, Massachusetts Institute of Technology, Cambridge, MA 02139)

The relative importance of Biot type flow and "squirting" mechanisms in determining the overall attenuation in saturated sandstones at various frequencies and pressures is studied. Elastic properties for a multiphase medium are found using the technique described in Toksöz et al. (1976). These moduli may be complex, introducing attenuation. Biot or inertial flow predicts an f^2 dependence for the attenuation coefficient at frequencies below that of Poisseuille flow breakdown and an $f^{1/2}$ dependence above. The contribution due to this mechanism is found using a formulation of Biot theory adapted by Stoll and Bryan (1970). "Squirting" flow involves the relative change in volume between connected cracks. The attenuation is found by introducing a complex fluid bulk modulus determined by the relaxation time for the flow. The critical frequency for this mechanism is in the sonic range. Another related mechanism, viscous shear relaxation, is of importance only at very high frequencies (> 1 MHz) for pore fluids of 1 cp viscosity.

Theoretical calculations of each mechanism for the Berea sandstone are carried out based on ultrasonic attenuation measurements as functions of differential pressure. It is concluded that for this case, fluid flow plays a secondary role relative to other attenuation mechanisms such as friction across cracks and grain boundaries. At these ultrasonic frequencies and relatively high pressures prior to pore collapse, Biot flow plays a more important role.

Stoll and Bryan, 1970, J. Acoust. Soc. Am., 47, 1440-1447.
Toksöz et al., 1976, Geophysics, 41, 621-645.

Presented at: American Geophysical Union
Spring Annual Meeting
April, 1978
Miami Beach, Florida

ATTENUATION AND TRAVEL TIME DELAYS OF SHEAR WAVES BENEATH THE MID-ATLANTIC RIDGE FROM TRANSFORM EARTHQUAKES

James L. Muller
Jennifer Lynn Hall
Sean C. Solomon (all at: Dept. of Earth and Planetary Sci., Massachusetts Institute of Technology, Cambridge, MA 02139)

For earthquakes on ridge-ridge transform faults, the azimuthal variation of body-wave differential attenuation and travel-time delay may be used to explore the shallow structure of the transform and of the intersecting ridge crest segments. For the 13 February 1967 earthquake on the Gibbs transform, SH waves show much higher attenuation for paths beneath the ridge crest to the northwest than for other directions [Solomon, 1973] and the S wave travel-time delays also show a strong azimuthal dependence [Duschenes and Solomon, 1977]. We have repeated these two sets of measurements for a number of additional earthquakes on mid-Atlantic ridge transforms, including the Gibbs, Oceanographer, Romanche, and St. Paul's transforms. Within the uncertainties in the respective data sets, no clear direction dependence is apparent for azimuths near the transform strike for either SH differential attenuation or S wave delay for any of these additional events. Thus velocity and Q variations beneath young seafloor in general are either not as pronounced or not as extensive as those inferred from the results of the 13 February 1967 event, and either that segment of the Gibbs transform or that particular earthquake source may be anomalous.

Presented at: American Geophysical Union
Spring Annual Meeting
April, 1978
Miami Beach, Florida

SIMULTANEOUS INVERSION OF SURFACE WAVE PHASE VELOCITY AND ATTENUATION: RAYLEIGH AND LOVE WAVES OVER CONTINENTAL AND OCEANIC PATHS

Wook Bae Lee* and Sean C. Solomon
Department of Earth & Planetary Sciences
Massachusetts Institute of Technology
Cambridge, MA 02139

*Current Address: Department of Earth & Space Sciences
University of California
Los Angeles, CA 90024

Submitted to Bulletin of the Seismological Society of America
May 1978
Revised September 1978

ABSTRACT

A formalism for the simultaneous inversion of surface wave phase velocity and attenuation, previously developed for Love waves, is extended in this paper to Rayleigh waves. The simultaneous inversion technique permits the specification of the intrinsic dispersion-attenuation relation that arises from linearity and causality, and takes full account of the dependence of surface wave phase velocity and Q^{-1} on the real and imaginary parts of an anelastic earth structure. The formalism, including resolution analysis and extremal inversion, is applied to combined Love and Rayleigh wave data sets for a tectonically active and a stable continental path and to Rayleigh wave data for a stable oceanic path. The depth to the low Q zone is 60 ± 20 km for the central Pacific, 80 ± 20 km for western North America, and 130 ± 30 km for east-central North America. Q^{-1} within the low-Q, low-velocity zone, however, is greater beneath western North America than beneath the central Pacific; the low-Q zone beneath east-central North America need not be a low velocity zone at frequencies above 1 Hz. The surface wave data cannot distinguish among several possible intrinsic dispersion-attenuation relations for the upper mantle.

INTRODUCTION

There are several advantages to the simultaneous treatment of phase velocity and Q^{-1} data in the inverse problem for surface wave dispersion and attenuation. The two data sets are coupled because both depend on the complete anelastic structure of the earth. More fundamentally, if linearity holds for seismic waves, a reasonable assumption at the small seismic strain amplitudes (less than 10^{-6})., then there is a predictable relation between local body wave phase velocity and attenuation. In particular, the principle of causality leads to an anelastic dispersion in solids which depends in detail on the magnitude and frequency dependence of attenuation (Lomnitz, 1957; Futterman, 1962; Jeffreys, 1965; 1975; Carpenter and Davies, 1966; Randall, 1976; Liu et al., 1976; Kanamori and Anderson, 1977). Eventual isolation of the physical mechanisms which control attenuation and anelastic dispersion in the mantle can result only by simultaneous consideration of phase velocity and Q^{-1} data. In an earlier paper (Lee and Solomon, 1978; hereinafter called Paper I), we presented a formalism for simultaneous inversion of phase velocity and Q^{-1} for Love waves, including the effect of anelastic dispersion, and we applied the formalism to data from western North America. An essentially equivalent treatment for Love waves without anelastic dispersion has been derived independently by Silva (1978). In this paper,

we extend the inversion formalism of Paper I to Rayleigh waves, and we apply it to combined Rayleigh and Love wave data sets in western and eastern North America and to Rayleigh wave data in the central Pacific.

An approximate correction to surface wave phase velocities or to normal mode periods to account for anelastic dispersion has been given by Carpenter and Davies (1966), Randall (1976), and Liu et al. (1976). Using this correction and the assumption of Q^{-1} independent of frequency over the seismic wave band, Anderson et al. (1977), Anderson and Hart (1976) and Hart et al. (1976, 1977) inverted corrected normal mode periods to derive frequency-dependent velocity models for the earth. An important result of their work is the removal of the 'baseline discrepancy' between earth models derived from short-period body wave data and models derived from long period free oscillations. The simultaneous inversion procedure presented in this paper differs formally from the approximate correction technique and leads to somewhat different results even for the velocity structure except in the limit of a narrow frequency band for both data and earth models of interest (Paper I; Lee, 1977).

In the sections to follow, we first extend to Rayleigh waves the formalism of Paper I for simultaneous inversion of phase velocity and Q^{-1} data to obtain a complex

frequency dependent earth model. The theoretical basis for the formalism is the generalization of Haskell's (1953) matrix treatment to anelastic structures by Schwab and Knopoff (1971, 1972). Resolving length analysis and extremal inversion (Lee and Solomon, 1975) are applied to Love and Rayleigh wave data sets over stable and tectonically active portions of North America and to Rayleigh wave data in the Pacific (Mitchell et al., 1976). Of interest are both the differences in the results between simultaneous inversion and previous separate inversions of velocity or Q^{-1} data sets and the implications of the different anelastic structural models for lithosphere and asthenosphere for the various paths sampled.

FORWARD PROBLEM

The problem of surface wave propagation through perfectly elastic multilayered media can be treated by the matrix formulation of Haskell (1953). In each layer, with boundary conditions of the free surface and of continuity of stress and displacement at the interfaces, a set of equations hold:

$$(\lambda_j + 2\mu_j)\,\nabla_t^2\,\phi_j = \rho_j \frac{\partial^2 \phi_j}{\partial t^2}$$

$$\mu_j\,\nabla_t^2\,\psi_j = \rho_j \frac{\partial^2 \psi_j}{\partial t^2} \qquad (1)$$

$$\mu_j \nabla_t^2 v_j = \rho_j \frac{\partial^2 v_j}{\partial t^2}$$

where $\nabla_t^2 = \frac{\partial}{\partial x^2} + \frac{\partial}{\partial z^2}$

$$u_j = \frac{\partial \phi_j}{\partial x} + \frac{\partial \psi_j}{\partial z}, \quad w_j = \frac{\partial \phi_j}{\partial z} - \frac{\partial \psi_j}{\partial x}$$

where x (propagation direction) and z are the horizontal and vertical axes, respectively, λ_j, μ_j and ρ_j are Lame parameters and density in the j-th layer, ψ_j and ϕ_j are potentials of the elastic field of the jth layer, and u_j, v_j, w_j are the displacements in the x, y, and z directions. For an anelastic (or viscoelastic) medium, the wave equation (1) and the solution have the same form in the frequency domain as for an elastic medium except that the elastic modulus is replaced with a complex quantity according to the 'correspondence principle' (Christensen, 1971). The Fourier transform of equation (1) with complex modulus is

$$E_j^*(\omega) \nabla_t^2 \bar{F}_j = \rho_j \omega^2 \bar{F}_j(x,z,\omega) \qquad (2)$$

where $\bar{F}_j(x,z,\omega) = \frac{1}{2\pi} \int_{-\infty}^{\infty} F_j(x,z,t)\, e^{i\omega t}\, dt$

where $E^*_j(\omega)$ represents either $\lambda_j + 2\mu_j$ or μ_j, F_j

represents ϕ_j, ψ_j or v_j, and $\bar{F}_j$ is the Fourier transform of F_j. $E_j^*(\omega)$ depends upon frequency in general. The frequency dependence can be specifically defined by the creep function (or relaxation function) of the medium. The solution to equation (2) for $F_j = v_j$ (for Love waves) with the boundary conditions mentioned above is given in Paper I. In analogous fashion, Haskell's matrix formulation may be extended to lossy media for Rayleigh waves as well as Love waves by implementing complex velocities and a dispersion relation between the real and imaginary parts of the intrinsic velocity.

INVERSE PROBLEM

The phase velocity and attenuation of surface waves on a multilayered, anelastic earth are obtained from the roots of the complex dispersion-attenuation functions (Schwab and Knopoff, 1971) f_L (Love) and f_R (Rayleigh):

$$f_L(T_i, c_i^L, \beta_j^*, \rho_j, d_j) = 0$$

$$f_R(T_i, c_i^R, \beta_j^*, \alpha_j^*, \rho_j, d_j) = 0 \qquad (3)$$

$$i = 1, 2, \ldots, m; \; j = 0,1,2,\ldots,n$$

where T_i, c_i^L, and c_i^R are ith period and Love and Rayleigh wave phase velocities and α_j, β_j and d_j are, respectively, the P- and S-wave velocities, density and thickness for the

jth layer (j=0 is the water layer for Rayleigh waves over oceanic paths). The velocities c^L, c^R, α^* and β^* are complex quantities.

The inverse problem consists of finding an anelastic (complex) earth model from given observational data pairs, phase velocities and phase attenuations. We start with an initial anelastic earth model and a set of observed dispersion-attenuation data pairs. The phase velocity and attenuation for the initial complex model are then calculated theoretically by Haskell's (1953) method at the period of each observed data pair. The generalized Haskell formulation is for a flat earth, whereas the observations are for a spherical earth. The flat-to-spherical transformation of Biswas and Knopoff (1970), as amended by Schwab and Knopoff (1971) to include anelasticity, is used for sphericity corrections for Love waves. For Rayleigh waves, a similar transform is given by Schwab and Knopoff (1972), though such a treatment is difficult to use in a computer code. In this study, Bolt and Dorman's (1961) empirical correction has been used to account for sphericity and gravity for complex phase velocity. Although the empirical correction has been tested only for the perfectly elastic case, it is probably sufficiently accurate for our purposes. North and Dziewonski (1976) improved this correction, but we did not adopt their improvement because only a minimal change is expected at the periods used here (<100 sec).

From the dispersion-attenuation calculations we also obtain the partial derivatives of the complex phase velocity c with respect to each complex parameter p of the layered earth

model. Then the initial perturbation equation can be written relating the desired parameter corrections to the differences between the corresponding theoretical and observed phase velocity values:

$$\Delta c_i^{L,R} = \frac{\partial c_i^{L,R}}{\partial p_j} \Delta p_j \qquad (4)$$

where the repeated indices imply summation for n layers. A similar equation for each period can be formed.

Because the physical significance of a complex quantity is more easily understood by decomposition into real and imaginary parts, we write equation (4) as two real equations, rather than one complex equation:

$$\underset{i}{\begin{pmatrix} \Delta c_1^{L,R} \\ \Delta c_2^{L,R} \end{pmatrix}} = \underset{ij}{\begin{pmatrix} \frac{\partial c_1^{L,R}}{\partial p_1} & \frac{\partial c_1^{L,R}}{\partial p_2} \\ \frac{\partial c_2^{L,R}}{\partial p_1} & \frac{\partial c_2^{L,R}}{\partial p_2} \end{pmatrix}} \underset{j}{\begin{pmatrix} \Delta p_1 \\ \Delta p_2 \end{pmatrix}} \qquad (5)$$

where $c_1^{L,R}$ and $c_2^{L,R}$ are the real and imaginary parts of $c^{L,R}$ and p_1 and p_2 are the real and imaginary parts of p.

It is assumed that all the dissipation is due to imperfect elasticity. By requiring the density to be real we ignore the possibility of losses due to imperfect inertia (Anderson and Archambeau, 1964). For Love waves we can write equation (5) in the form:

$$\begin{pmatrix} \Delta c_1^L \\ \Delta c_2^L \end{pmatrix}_i = \begin{pmatrix} \frac{\partial c_1^L}{\partial \beta_1} & \frac{\partial c_1^L}{\partial \beta_2} & \frac{\partial c_1^L}{\partial \rho} \\ \frac{\partial c_2^L}{\partial \beta_1} & \frac{\partial c_2^L}{\partial \beta_2} & \frac{\partial c_2^L}{\partial \rho} \end{pmatrix}_{ij} \begin{pmatrix} \Delta \beta_1 \\ \Delta \beta_2 \\ \Delta \rho \end{pmatrix}_j \qquad (6)$$

where β_1 and β_2 are the real and imaginary parts of the shear wave velocity in the jth layer. For Rayleigh waves, equation (5) can be written as

$$\begin{pmatrix} \Delta c_1^R \\ \Delta c_2^R \end{pmatrix}_i = \begin{pmatrix} \frac{\partial c_1^R}{\partial \beta_1} & \frac{\partial c_1^R}{\partial \beta_2} & \frac{\partial c_1^R}{\partial \alpha_1} & \frac{\partial c_1^R}{\partial \alpha_2} & \frac{\partial c_1^R}{\partial \rho} \\ \frac{\partial c_2^R}{\partial \beta_1} & \frac{\partial c_2^R}{\partial \beta_2} & \frac{\partial c_2^R}{\partial \alpha_1} & \frac{\partial c_2^R}{\partial \alpha_2} & \frac{\partial c_2^R}{\partial \rho} \end{pmatrix}_{ij} \begin{pmatrix} \Delta \beta_1 \\ \Delta \beta_2 \\ \Delta \alpha_1 \\ \Delta \alpha_2 \\ \Delta \rho \end{pmatrix}_j \qquad (7)$$

Since one or both of $\Delta\beta_1$ and $\Delta\beta_2$ depend upon frequency (as do $\Delta\alpha_1$ and $\Delta\alpha_2$ for Rayleigh waves), the right hand sides of equations (6) and (7) should be standardized at a single reference frequency for inversion (see below). Generalizing equation (4) to m complex observations and using matrix

notation gives:

$$\underset{\sim}{A}^{L,R}\ \underset{\sim}{x}^{L,R} = \underset{\sim}{y}^{L,R} \tag{8}$$

where $\underset{\sim}{y}$ is an m x 1 matrix of differences between observed and predicted phase velocities and attenuations, $\underset{\sim}{A}$ is an m x n matrix of partial derivatives, and $\underset{\sim}{x}$ is an n x 1 matrix of perturbations to the starting anelastic earth model. The elements of $\underset{\sim}{y}^{L}$, $\underset{\sim}{A}^{L}$ and $\underset{\sim}{x}^{L}$ are real 2 x 1, 2 x 3 and 3 x 1 matrices, respectively and the elements of $\underset{\sim}{y}^{R}$, $\underset{\sim}{A}^{R}$ and $\underset{\sim}{x}^{R}$ are real 2 x 1, 2 x 5 and 5 x 1 matrices, respectively.

The partial derivatives of phase velocity with respect to shear velocity are obtained by implicit function theory (Schwab and Knopoff, 1972):

$$\frac{\partial c^{L,R}}{\partial \beta^*} = -\frac{\partial f_{L,R}}{\partial \beta^*} \Big/ \frac{\partial f_{L,R}}{\partial c^{L,R}}$$

$$\frac{\partial c^{R}}{\partial \alpha^*} = -\frac{\partial f_{R}}{\partial \alpha^*} \Big/ \frac{\partial f_{R}}{\partial c^{R}} \tag{9}$$

where f_L, given in Paper I, and

$$f_R = T^{(o)}\overline{F}^{(1)}F^{(2)} \cdots \begin{cases} F^{(n-2)}\overline{F}^{(n-1)}T^{(n)} & \text{even n} \\ \overline{F}^{(n-2)}F^{(n-1)}\overline{T}^{(n)} & \text{odd n} \end{cases}$$

are the dispersion-attenuation functions for Love and Rayleigh waves, and where $T^{(o)}$, $T^{(n)}$, $F^{(j)}$, and $\overline{F}^{(j)}$ are given in Schwab and Knopoff (1972). The partial derivatives required to evaluate equation (9) are given for Love waves in Paper I. For Rayleigh

waves, define

$$\overline{\Delta}^{(n-1)} = \overline{F}^{(1)}F^{(2)}\overline{F}^{(3)}\ldots F^{(n-2)}\overline{F}^{(n-1)}$$

$$\Delta^{(n-1)} = \overline{F}^{(1)}F^{(2)}\overline{F}^{(3)}\ldots \overline{F}^{(n-2)}F^{(n-1)}$$

Then

$$f_R = \begin{cases} T^{(o)}\,\overline{\Delta}^{(n-1)}T^{(n)} & \text{for even } n \\ T^{(o)}\,\Delta^{(n-1)}\overline{T}^{(n)} & \text{for odd } n \end{cases}$$

For even n,

$$\frac{\partial f_R}{\partial c^R} = \frac{\partial T^{(o)}}{\partial c^R}\,\overline{\Delta}^{(n-1)}T^{(n)} + T^{(o)}\,\frac{\partial \overline{\Delta}^{(n-1)}}{\partial c^R}T^{(n)} + T^{(o)}\overline{\Delta}^{(n-1)}\frac{\partial T^{(n)}}{\partial c^R} \qquad (10)$$

where

$$\frac{\partial \overline{\Delta}^{(n-1)}}{\partial c^R} = \sum_{j=1}^{n-1} F^{(1)}\overline{F}^{(2)}\ldots\frac{\partial F^{(j)}}{\partial c^R}\ldots\overline{F}^{(n-1)}T^{(n)}$$

and

$$\frac{\partial f_R}{\partial p_j} = T^{(o)}\overline{F}^{(1)}F^{(2)}\ldots\frac{\partial F^{(j-1)}}{\partial p_j}\ldots\overline{F}^{(n-1)}T^{(n)}$$

$$+ T^{(o)}\overline{F}^{(1)}F^{(2)}\ldots\frac{\partial F^{(j)}}{\partial p_j}\ldots\overline{F}^{(n-1)}T^{(n)}$$

$$j = 2, 3, \ldots, n-1$$

$$\frac{\partial f_R}{\partial p_n} = T^{(o)}\overline{F}^{(1)}F^{(2)}\cdots\frac{\partial \overline{F}^{(n-1)}}{\partial p_n}T^{(n)} + T^{(o)}\overline{F}^{(1)}F^{(2)}\cdots\overline{F}^{(n-1)}\frac{\partial T^{(n)}}{\partial p_n}$$

$$\frac{\partial f_R}{\partial p_1} = \frac{\partial T^{(o)}}{\partial p_1}\overline{F}^{(1)}F^{(2)}\cdots\overline{F}^{(n-1)}T^{(n)} + T^{(o)}\frac{\partial \overline{F}^{(1)}}{\partial p_1}F^{(2)}\cdots\overline{F}^{(n-1)}T^{(n)}$$

and where p can be either α or β. For odd n, similar formulae hold.

Since $c^L = c^L(\beta^*)$ and $c^R = c^R(\alpha^*,\beta^*)$ are analytic, single-valued functions (their first derivatives are unique and independent of the direction along which the derivative is taken), the Cauchy-Riemann condition is satisfied for

$$c^{L,R} = c_1^{L,R} + ic_2^{L,R}, \quad \beta^* = \beta_1 + i\beta_2, \quad \alpha^* = \alpha_1 + i\alpha_2$$

(Morse and Feshbach, 1953, p. 357), and

$$\frac{\partial c_1^{L,R}}{\partial \beta_1} = \frac{\partial c_2^{L,R}}{\partial \beta_2}, \qquad \frac{\partial c_1^{L,R}}{\partial \beta_2} = -\frac{\partial c_2^{L,R}}{\partial \beta_1} \tag{11}$$

$$\frac{\partial c_1^{R}}{\partial \alpha_1} = \frac{\partial c_2^{R}}{\partial \alpha_2}, \qquad \frac{\partial c_1^{R}}{\partial \alpha_2} = -\frac{\partial c_2^{R}}{\partial \alpha_1}$$

From equation (11), only four of the elements of the 2 x 3 real matrix in equation (6) are independent for Love waves and only six of the elements of the 2 x 5 real matrix in equation (7) are independent for Rayleigh waves. Thus the matrices can be completely specified from the real and imaginary parts of $\partial c^{L,R}/\partial\beta^*$ and $\partial c^{R}/\partial\alpha^*$ and from $\partial c^{L,R}/\partial\rho$.

RESOLUTION

As in Paper I, we follow the treatment of Der and Landisman (1972) for parameter resolution for a two-parameter (β_1,β_2) earth model. The linear combination of data $y_i^{L,R}$ used as the estimator of a desired parameter $x_k^{L,R}$ in layer k is

$$x_k^{L,R} = \sum_i r_{ik} y_i^{L,R} = \sum_i^N \sum_j^M r_{ik} S_{ij}^{L,R} x_j^{L,R} \qquad (12)$$

where r_{ik} is a coefficient to be determined, N is the number of data, M is the number of layers in the model, and where

$$S_{ij} = \frac{\partial y_i^{L,R}}{\partial x_j^{L,R}}, \qquad (13)$$

normalized by the layer thickness in kilometers.

The three quantities to be minimized are (Der and Landisman, 1972)

1) the variance of the desired variable $x_k^{L,R}$
2) s_1, the resolution for $x_k^{L,R}$
3) s_2, the dependence on the undesired variable $\bar{x}_k^{L,R}$ for the same layer.

If we assume that the observational errors are independent

$$\text{var } x_k^{L,R} = \sum_i^N r_{ik}^2 \text{ var } y_i^{L,R}$$

$$(s_1^{L,R})^2 = \sum_{j=k}^M d_j (E_{kj}^{L,R})^2 \qquad (14)$$

$$(s_2^{L,R})^2 = \sum_j^M d_j (F_{kj}^{L,R})^2$$

where d_j is the layer thickness and

$$E_{kj}^{L,R} = \sum_i^N r_{ik} S_{ij}^{L,R} \qquad (15)$$

$$F_{kj}^{L,R} = \sum_i^N r_{ik} T_{ij}^{L,R}, \quad T_{ij}^{L,R} = \frac{\partial y_i^{L,R}}{\partial \bar{x}_j}$$

These three objectives can be accomplished by minimizing the function

$$\epsilon_k^{L,R} = \sin\xi \text{ var } x_k^{L,R} + \cos\xi\sin\eta (s_1^{L,R})^2 + \cos\xi\cos\eta (s_2^{L,R})^2 + 2\theta (E_{kk}^{L,R} - 1) \qquad (16)$$

where θ is a Lagrange multiplier. The parameters ξ and η ($0 \leq \xi, \eta \leq \pi/2$) are adjusted so as to balance the three desired minimizations. As ξ is increased, the approximation to the delta function becomes poorer, the variances of $x_k^{L,R}$ become smaller and separation between $x_k^{L,R}$ and

$\bar{x}_k^{L,R}$ improves.

Resolution analysis should strictly be conducted with density as a third independent parameter, since density is included in the inversions presented in this paper. With no additional data, such as from higher modes, the resolution for β_1 and β_2 would be worse than for the examples shown below.

DISPERSION-ATTENUATION RELATIONS

Dispersion-attenuation relations can be given in two different forms. In the frequency domain, for a given frequency dependence of Q, Kramers-Krönig relations provide this relation. A frequency dependence or independence of Q can be specified by a superposition of individual relaxation mechanisms or viscoelastic elements, or by empirical observations. In the time domain, Boltzmann's after-effect equation will provide a complex modulus and a dispersion relation for a given creep function or relaxation function. A creep (or relaxation) function can similarly be given by superposing the creep (or relaxation) function of each viscoelastic element using a distribution function, or by empirical observations. No matter which procedure is used, the same dispersion-attenuation relations are given for the same frequency dependence of Q. We discuss the two categories of frequency independent and frequency dependent Q separately.

Frequency independent Q. Various attempts have been made to explain the apparently nearly constant Q in the seismic frequency band (Futterman, 1962; Lomnitz, 1957; Azimi et al., 1968; Liu et al., 1976). Futterman (1962) and Azimi et al. (1968) derived

dispersion relations in the frequency domain:

$$\chi(\omega) = \begin{cases} C_1\omega & \text{(Futterman)} \\ \dfrac{\chi_o\omega}{1 + \chi_1\omega} & \text{(Azimi } \underline{\text{et}} \text{ } \underline{\text{al.}}\text{)} \end{cases} \tag{17}$$

where $\chi(\omega)$ is the attenuation coefficient, or the imaginary part of the complex wave number, and C_1, χ_o, χ_1 are constants. Equations (17) give the following dispersion relations:

$$v(\omega)/v_\infty = \begin{cases} \left[1 - \dfrac{2C_1 v_\infty}{\pi} \ln\omega\right]^{-1} & \text{(Futterman)} \\ \left[1 - \dfrac{2\chi_o v_\infty}{\pi(1-\chi_1^2\omega^2)} \ln(\chi_1\omega)\right]^{-1} & \text{(Azimi } \underline{\text{et}} \text{ } \underline{\text{al.}}\text{)} \end{cases} \tag{18}$$

where v_∞ is the non-dispersive limit of v and where χ_1 is chosen so that $\chi(\omega)$ is almost linear in some finite frequency range of interest $0 \leq \omega \leq \omega_{lim}$ (Azimi et al. used the value 10^{-7} sec for the constant χ_1).

For attenuation

$$Q^{-1}(\omega) = \begin{cases} 2C_1 v_\infty & \text{(Futterman)} \\ \dfrac{2\chi_o v_\infty}{1 + \chi_1\omega} & \text{(Azimi } \underline{\text{et}} \text{ } \underline{\text{al.}}\text{)} \end{cases}$$

Since χ_1 is very small (10^{-7}), these two expressions are nearly identical.

Lomnitz (1957) and Liu et al. (1976) instead derived dispersion relations in the time domain. The creep function was given as follows:

$$\phi(t) = \begin{cases} q \ln(1 + at) & \text{(Lomnitz)} \\ C \int_{\tau_1}^{\tau_2} (1-e^{-t/\tau}) d\tau/\tau & \text{(Liu et al.)} \end{cases} \tag{19}$$

where q, a, and C are constants and τ is a relaxation time. These creep functions give the following dispersion relations

$$v(\omega)/v_\infty = \begin{cases} 1 + q/2[\gamma + \ln \frac{\omega}{a}] & \text{(Lomnitz)} \\ 1 + C/2 \ln(\omega\tau_1) & \text{(Liu et al.)} \end{cases} \tag{20}$$

where γ is a constant, and 1/Q is approximately constant at the value $q\pi/2$ or $C\pi/2$, respectively. From (18) and (20), when $Q^{-1} \simeq Q_o^{-1}$ is small,

$$v(\omega_1)/v(\omega_2) = 1 + \frac{1}{\pi Q_o} \ln \left(\frac{\omega_1}{\omega_2}\right) \tag{21}$$

This is a good approximation for various attenuation laws of constant or nearly constant Q.

Frequency dependent Q. Jeffreys (1958) modified equation (19) of Lomnitz (1957) to the Jeffreys-Lomnitz law, which also represents the empirical relation of Andrade (1911). The creep function for the Jeffreys-Lomnitz law is

$$\phi(t) = q/\nu \; [(1 + at)^{\nu} - 1] \qquad (22)$$

where q and a are constants and ν is a number between 0 and 1. As ν goes to zero, (22) tends toward the original Lomnitz Law. In the frequency domain, the creep function (22) gives the following dispersion relations

$$\begin{aligned} Q^{-1}(\omega) &= q\, a^{\nu}(\nu-1)!\; \omega^{-\nu} \sin \frac{\pi\nu}{2} \\ v(\omega)/v_{\infty} &= \left[1 + \frac{Q^{-1}}{2} \cot \frac{\pi\nu}{2}\right]^{-1} \end{aligned} \qquad (23)$$

(Jeffreys and Crampin, 1960; Jeffreys, 1965, 1975). A number of suggestions for the proper value of ν have been made by Jeffreys (1/4, 1/5) and Andrade (1/3). Lamb (1962), Strick (1967) and Azimi et al. (1968) considered the following frequency dependence of the attenuation coefficient:

$$\chi(\omega) = C_2\, \omega^{1-\nu} \qquad (24)$$

where ν is a number between 0 to 1.

The frequency domain approach gives the following dispersion relations from (24) (Paper I):

$$Q^{-1}(\omega) = 2C_2 v_\infty \omega^{-\nu}$$

$$v(\omega)/v_\infty = [1 + C_2 v_\infty \omega^{-\nu} \cot \frac{\pi\nu}{2}]^{-1} \qquad (25)$$

which is identical to (23) for suitable choice of C_2. Lamb (1962) used $\nu = 1/2$ and Strick (1967) and Azimi et al. (1968) attempted to account for nearly constant Q with $\nu = 0.078$ (Strick) and $\nu = 0.1$ (Azimi et al.).

Equations (23) and (25) give

$$Q^{-1}(\omega_1)/Q^{-1}(\omega_2) = (\omega_1/\omega_2)^{-\nu}$$

$$\frac{v(\omega_1)}{v(\omega_2)} = [1 + \frac{Q_o^{-1}}{2} \cot \frac{\pi\nu}{2} (1 - \frac{\omega_1}{\omega_2})^{-\nu}]^{-1} \qquad (26)$$

where $Q_o^{-1} = Q^{-1}(\omega_2)$.

Other dispersion-attenuation relations are possible with different frequency dependence for $v(\omega)$ and $Q^{-1}(\omega)$; for instance, the relation for a standard linear solid is given in Zener (1948). Only relations (21) and (26) will be used, however, in the inversions below.

INVERSION PROCEDURES

For the dispersion-attenuation relations, Q_β^{-1}, Q_α^{-1}, and the real body-wave phase velocities β and α are related to β_1, β_2, α_1 and α_2 such that

$$Q_\beta^{-1} = 2\beta_2/\beta_1 \qquad (27)$$

$$Q_\alpha^{-1} = 2\alpha_2/\alpha_1$$

$$\beta = (\beta_1^2 + \beta_2^2)/\beta_1$$

$$\alpha = (\alpha_1^2 + \alpha_2^2)/\alpha_1$$

For each of these relations, β_1, α_1 or all β_1, β_2, α_1 and α_2 depend on frequency

$$\beta_{1j}(\omega_i) = \bar{\beta}_{1j} + g(\omega_i)\bar{\beta}_{2j}$$

$$\beta_{2j}(\omega_i) = \bar{\beta}_{2j}\, h(\omega_i) \qquad (28)$$

$$\alpha_{1j}(\omega_i) = \bar{\alpha}_{1j} + g(\omega_i)\bar{\alpha}_{2j}$$

$$\alpha_{2j}(\omega_i) = \bar{\alpha}_{2j}\, h(\omega_i)$$

where g and h are specified functions of frequency and $\bar{\beta}_{1j}$, $\bar{\beta}_{2j}$, $\bar{\alpha}_{1j}$ and $\bar{\alpha}_{2j}$ are values of β_{1j}, β_{2j}, α_{1j} and α_{2j} at a reference frequency, respectively. In general, the inverse problem to equation (8) is conducted at the reference frequency, the partials in (6) and (7) are with respect to $\bar{\beta}_1$, $\bar{\beta}_2$, $\bar{\alpha}_1$, and $\bar{\alpha}_2$, and the earth structure at any other frequency follows from (28) (see Appendix).

DATA

The data sets for Q_L^{-1} and Q_R^{-1} for North American paths are described and tabulated in Lee and Solomon (1975). The accompanying phase velocity measurements are given in Solomon (1971). The western North American path crosses primarily the tectonically active Basin and Range physiographic province. The east-central North American path crosses primarily the tectonically quiet Great Plains and Central Lowlands physiographic provinces. The Q^{-1} data were also analyzed from a different viewpoint by Solomon (1972a,b).

The data set for Q_R^{-1} for the central Pacific Ocean is a subset of that given by Mitchell *et al.* (1976). These workers determined Q_R^{-1} from the records of three earthquakes at WWSSN stations distributed around the west coast of America, the Far East and the Pacific. The measurements represent a weighted average of the entire Pacific Ocean region. Such an average does not strictly represent the structure in any particular location because of the lateral variation of oceanic structure with the age of the sea floor (Forsyth, 1975).

We have chosen one event among the three for which the data sample paths predominantly within the relatively old (80-90 m.y. average age) central Pacific. The locations of the event (April 26, 1973, $20^h26^m30.8^s$, latitude 19.9°N, longitude 155.13°W, m_b = 6.0), stations and paths are shown in Figure 1.

The corresponding phase velocity curve is taken to be a weighted average of 'pure path' velocities, calculated using the published magnetic anomalies (Pitman et al. 1974) for the Pacific and the results of Forsyth (1975, 1977) on the variation of phase velocity with sea floor age. We divided the Pacific region into eleven age zones plus continents (Table 1). Each great circle path from event to station was plotted on the map of age zone boundaries, from which we calculated the total path length in each age group for the sum of all the paths. Then the weighted average of phase velocity and group velocity at each period were determined using the pure-path results of Forsyth (1975, 1977), interpolating where necessary, and the weights shown in the Table 1. The resultant weighted phase velocity curve for the central Pacific, appropriate to the Q_R^{-1} data set of Mitchell et al. (1976), is shown in Figure 2.

The magnetic anomaly map on the basis of which seafloor ages were estimated does not include the marginal basins of the western Pacific, across which pass many of

the surface wave paths used here. Additional age information for these basins have been taken from Weissel (1977) for the Lau Basin, from Weissel et al. (1977) for the Coral Sea and New Hebrides Basin, from Watts et al. (1977) for the south Fiji Basin and from Sclater et al. (1976) for the Philippine Sea.

INVERSIONS

Love and Rayleigh waves in western North America. The starting models for calculation of partial derivatives for western North America are listed in Table 2 for Q independent of frequency. The models for β and Q_β^{-1} are taken from Paper I. For Q independent of frequency (and for other dispersion-attenuation relations) the starting models are determined by averaging the extreme models of β and Q_β^{-1} as functions of depth. The density model remains real but is allowed to vary in the inversion process. The P-wave velocity (Table 2) is chosen to have features similar to model CIT 111 of Archambeau et al. (1969) and is held fixed during the inversion, since surface wave phase velocity is least sensitive to changes in α among (α,β,ρ) and thus the resolution of the inverse problem is poor for α. Because of the large uncertainties in measured Q^{-1}, we will assume that losses under purely compressive stress are negligible, i.e. $Q_\alpha^{-1} = 4/3(\beta/\alpha)^2 Q_\beta^{-1}$. Finally, a 2 km sedimentary layer has been added to improve the fit for Rayleigh wave phase velocity. For purposes of calculating partial derivatives, the equivalent flat model to that in

Table 2 was divided into 28 layers and an underlying halfspace.

The cross-partial elements of the partial derivative matrix (see equation 7) for Rayleigh waves, $\partial c_1^R/\partial\beta_2$, are an order of magnitude smaller than those for Love waves (Figure 3; c.f., Paper I). This result means that the difference between simultaneous inversion and the correction technique of Anderson et al. (1977) and others is less significant for Rayleigh waves than for Love waves. However, the advantage of simultaneous inversion still remains because the changes in the Q^{-1} model itself are sensitive to the result of the velocity model inversion.

Resolution analysis was conducted as described above. The optimal averaging kernels E_{kj} (equation 15) for both Love and Rayleigh waves are shown in Figure 4 for five layers. As in Paper I, a 5-layer model is adopted for the inversions.

External inversion has been carried out using the linear programming technique adopted in Lee and Solomon (1975) and in Paper I. Envelopes in model space of β_1, β_2, and ρ are determined from the observational data and their uncertainties and from the constraints that the model parameters lie within certain a priori bounds. During inversions, the shear velocity and attenuation and the density in the top sedimentary layer and in the half space have been held fixed.

The envelopes of shear velocity β, attenuation Q_β^{-1}, and density ρ are given in Table 3 and Figure 5 for a model (S31W) with Q independent of frequency, and for models (S32W, S33W) with

Q varying as a power of the frequency (ν = 1/5 and 1/2, respectively). The corresponding envelopes in data space are illustrated for these models in Figures 6-9. A 1 Hz reference frequency is used for all models.

Love and Rayleigh waves in east-central North America. The starting models of α,β, ρ and Q^{-1} for east-central North America are listed in Table 4. The models of α, β and ρ are adapted from the results of McEvilly (1964) and the Q_β^{-1} model for the constant-Q inversion is from Lee and Solomon (1975). The initial model Q_β^{-1} for inversion using a power law dependence of Q on frequency is chosen to be an acceptable solution to the separate Q inversion.

The averaging kernels E_{kj} from resolution analysis for both Love and Rayleigh waves are shown in Figure 10, for five layers. Four layers and a fixed-parameter halfspace were used in the inversions.

The envelopes of shear velocity β, attenuation Q_β^{-1} and density ρ are given in Table 5 and Figure 11 for a dispersion model (S31E) with Q independent of frequency and for a model (S32E) with Q varying as a power of frequency (ν=1/2). The corresponding envelopes in data space are illustrated for these models in Figures 12-15.

Rayleigh waves in the central Pacific. The starting models of α,β, ρ and Q_β^{-1} are listed in Table 6. The starting model for the crust is modified from the 'standard crustal section' of Forsyth (1975), in which 5 km of water layer, 0.2 km of sedimentary layer and 6.8 km of crustal layer are assumed. For the starting model of the mantle, the density is taken to be 3.4-3.5 g/cm^3, the S-wave velocity β is 4.35 km/sec in the low velocity zone (50-220 km) and 4.60 km/sec in the high velocity lid.

$\alpha \sim 1.7\beta$ (<220 km depth) and $\alpha \sim 1.8\beta$ (>220 km depth). The starting model for Q_β^{-1} is taken from Mitchell (1976). The averaging kernels E_{kj} for Rayleigh waves are shown in Figure 16 for four layers.

The envelopes of shear velocity β and shear attenuation Q_β^{-1} are given in Table 7 and in Figure 17 for a dispersion model (S21P) with Q independent of frequency. No test for the frequency dependence of Q has been performed since the Q_R^{-1} data are relatively poor. The corresponding envelopes in data space for model S21P are illustrated in Figures 2 and 18. The dashed lines in Figure 17 represent the average of the models defining the envelopes in model space. This averaged model provides a good fit to the data (Figures 2 and 18).

DISCUSSION

Love and Rayleigh waves in western North America. A problem in western North America may be SV/SH anisotropy. Love and Rayleigh wave phase velocities are incompatible, in the sense defined by Lee and Solomon (1975), for almost the entire common frequency range (Figures 6 and 7). Also as noted by Lee and Solomon (1975), Rayleigh wave attenuation Q_R^{-1} in the period range 35-40 seconds shows disagreement with Love wave attenuation Q_L^{-1}. This is not a consequence of simultaneous inversion but appears to be a consequence either of anisotropy or of some interference effects in the waveforms analyzed. The measurements of Rayleigh wave phase velocity in Solomon (1971) are

comparatively lower than other reported measurements in the western United States (Biswas and Knopoff, 1974). This may be a real effect, however; the contour map of P_n velocity in the western United States (Archambeau et al., 1969) shows that the path between LON and TUC lies in a low P_n velocity 'valley'.

In Paper I, the assumption of constant Q led to the removal of the requirement for a low velocity zone for shear at frequencies at or above 1 Hz. When Rayleigh as well as Love wave data are used, a low velocity zone at 1 Hz is a feature of all models resulting from the inversion. The low velocity zone and low Q zones coincide, a property that is preserved even when starting models with no low velocity zones are used in the inversion (Paper I).

Love and Rayleigh waves in east-central North America. The simultaneous inversion results for east-central North America give a thick lithosphere, or high velocity and high Q lid, and a monotonically increasing velocity model at 1 Hz. A low velocity zone may not be required at 1 Hz. However, a low Q zone is probably present at depths greater than 130 km.

For both sets of North American attenuation data, much of the data incompatibility in certain period ranges which occurred in the separate inversion for Q^{-1} (Lee and Solomon, 1975) does not arise in the simultaneous inversion. This is true in particular of the low Q^{-1} values near 20 to 25 sec period, a feature of other Q^{-1} data sets (Tryggvason, 1965; Tsai and Aki, 1969).

Another result of simultaneous inversion for both regions is that the S-wave velocities in the mantle are increased considerably and density is decreased compared to the results of separate inversion of phase velocity. At the same time,

for Q independent of frequency, Q_β^{-1} in the asthenosphere is greater than predicted by the results of separate inversion.

The frequency dependent Q_β^{-1} models are also satisfactory for predicting observations. To discriminate among the possible frequency dependencies of Q_β^{-1}, more precise measurements of Q_β^{-1} or of body wave dispersion must be made.

Rayleigh waves in the central Pacific. The results of simultaneous inversion for β and Q_β^{-1} in the central Pacific are shown in Figure 17. The low velocity zone and low Q zone coincide and are extensive (60 to 225 km depth). The lithospheric thickness is less than in both western North America (tectonic) and east-central North America (stable).

The result of simultaneous inversion (model S21P) shows a shear velocity profile generally similar to Forsyth's (1977) old ocean. While Forsyth suggested 70-90 km as the starting depth of partial melting, model S21P gives a slightly shallower asthenosphere at 60 km depth, in agreement with Mitchell (1976). This may be due to the influence of Q^{-1} on the velocity structure but is at least as likely due to the coarse layering and age-averaged data used in this study.

Compared with Mitchell's (1976) Q model, the noticeable differences in S21P are that the low Q zone may extend deeper than 220 km, though the Q structure at that depth is not well resolved, and that the low Q zone is more pronounced. At around 100 sec period, Mitchell's Q_R^{-1} data were incompatible.

CONCLUSIONS

We have extended the formalism (Paper I) for the simultaneous inversion of surface wave phase velocity and attenuation to Rayleigh waves. Simultaneous inversions of data for both Love and Rayleigh waves have been accomplished for tectonically active and stable continental paths and an inversion for Rayleigh wave data alone has been given for a stable ocean basin.

An important aspect of the simultaneous inversion is the incorporation of the intrinsic anelastic dispersion which results from linearity and causality. This intrinsic dispersion of shear velocity can be quite large within the low-Q zone beneath oceanic and tectonically active regions. Beneath western North America, for instance, dispersion can be as great as 10 percent over two decades in frequency, depending on the frequency dependence of Q^{-1}.

The simultaneous inversion technique presented here and in Paper I is formally different from the approximate inversion scheme of Anderson *et al.* (1977) and gives different results. These differences can be significant when the observational frequency band is wide and/or the reference frequency is far from the observational frequencies. No matter how the observational frequency band is spread, no matter where we choose a reference frequency, a given dispersion-attenuation relationship may be used to extrapolate models to any frequencies. The difference between the simultaneous

inversion approach and the simple correction of phase velocity for anelastic dispersion is larger for Love waves than for Rayleigh waves, because the cross partial derivatives for Rayleigh waves are much smaller than for Love waves. However, most of the advantages of simultaneous inversion are still retained for Rayleigh waves.

Other consequences of simultaneous inversion are that the incompatibility in the attenuation data set decreases substantially and that the resolution in Q^{-1} versus depth in the earth is improved for a given dispersion-attenuation relation over the separate inversion of Q^{-1} data alone.

Several possible intrinsic dispersion-attenuation relations were tested against the Love and Rayleigh wave phase velocity and Q^{-1} data sets for North American paths, including those for Q independent of frequency and Q varying as a small positive power of frequency. The available surface wave data sets do not discriminate among these relations. Probably the best prospect for choosing among them is in observing body wave dispersion (Jordan and Sipkin, 1977) or frequency dependence of Q (Solomon et al., 1970; Der and McElfresh, 1977).

The most interesting results of the inversions are the lateral variations of mantle structure. A distinctive low Q zone appears to exist everywhere we have data, including western North America (tectonically active continent), east-central North America (stable platform) and the central Pacific

(stable ocean basin). However, the thickness of the high-Q lid varies from place to place: 60±20 km in the central Pacific, 80±20 km in western North America and 130±30 km in east-central North America. These results are related to the differing tectonic history of each region. In east-central North America, a thick lithosphere has presumably grown over time, and the asthenosphere shows relatively mild attenuation and admits the possibility of no low velocity zone at a frequency of 1 Hz and above. In western North America, a thinner lithosphere with substantially higher attenuation in the asthenosphere is characteristic. Many authors have suspected there is substantial partial melting in the asthenosphere of this region. The excess heat necessary to produce melting may have been related to the recent subduction of oceanic lithosphere along western North America.

The low velocity and low Q zones coincide in western North America. The inversion of Love wave data alone (Paper I) shows that the assumption of Q independent of frequency over the entire seismic band leads to the removal of the requirement for a low velocity zone for shear waves at frequencies above 1 Hz. The low velocity zone persists at these frequencies, however, in the results of the combined inversion of Love and Rayleigh wave data. A possible anisotropy in western North America may have contributed to this result, though, as well as to an inability to discriminate among various dispersion-attenuation relations. In the Pacific,

the low velocity and low Q zones coincide as in western North America. The Pacific shows a thinner lithosphere (60 km thick) but lower shear attenuation Q_β^{-1} in the asthenosphere than in the tectonically active western North America.

APPENDIX

PARTIAL DERIVATIVES AT A REFERENCE FREQUENCY FOR RAYLEIGH WAVES

Using equation (28), partial derivatives at a reference frequency can be given as follows. For convenience, the symbols β_1^o, β_2^o, α_1^o, and α_2^o are used for β_1, β_2, α_1, α_2, respectively, at the reference frequency.

$$\left(\frac{\partial c_1}{\partial \beta_1^o}\right)_{ij} = \left(\frac{\partial c_1}{\partial \beta_1}\right)_{ij} \tag{A.1}$$

$$\left(\frac{\partial c_1}{\partial \beta_2^o}\right)_{ij} = \left(\frac{\partial c_1}{\partial \beta_1}\right)_{ij} g_i + \left(\frac{\partial c_1}{\partial \beta_2}\right)_{ij} h_i \tag{A.2}$$

$$\left(\frac{\partial c_2}{\partial \beta_1^o}\right)_{ij} = \left(\frac{\partial c_2}{\partial \beta_1}\right)_{ij} = -\left(\frac{\partial c_1}{\partial \beta_2}\right)_{ij} \tag{A.3}$$

$$\left(\frac{\partial c_2}{\partial \beta_2^o}\right)_{ij} = \left(\frac{\partial c_2}{\partial \beta_1}\right)_{ij} g_i + \left(\frac{\partial c_2}{\partial \beta_2}\right)_{ij} h_i \tag{A.4}$$

$$= -\left(\frac{\partial c_1}{\partial \beta_2}\right)_{ij} g_i + \left(\frac{\partial c_1}{\partial \beta_1}\right)_{ij} h_i$$

$$\left(\frac{\partial c_1}{\partial \alpha_1^o}\right)_{ij} = \left(\frac{\partial c_1}{\partial \alpha_1}\right)_{ij} \tag{A.5}$$

$$\left(\frac{\partial c_1}{\partial \alpha_2^o}\right)_{ij} = \left(\frac{\partial c_1}{\partial \alpha_1}\right)_{ij} g_i + \left(\frac{\partial c_1}{\partial \alpha_2}\right)_{ij} h_i \tag{A.6}$$

$$\left(\frac{\partial c_2}{\partial \alpha_1^o}\right)_{ij} = \left(\frac{\partial c_2}{\partial \alpha_1}\right)_{ij} = -\left(\frac{\partial c_1}{\partial \alpha_2}\right)_{ij} \tag{A.7}$$

$$\left(\frac{\partial c_2}{\partial \alpha_2^o}\right)_{ij} = \left(\frac{\partial c_2}{\partial \alpha_1}\right)_{ij} g_i + \left(\frac{\partial c_2}{\partial \alpha_2}\right)_{ij} h_i \tag{A.8}$$

$$= -\left(\frac{\partial c_1}{\partial \alpha_2}\right)_{ij} g_i + \left(\frac{\partial c_1}{\partial \alpha_1}\right)_{ij} h_i$$

The last steps of equation (A.3), (A.4), (A.7), and (A.8) are consequences of the Cauchy-Riemann relations (11). From dispersion relations (21) and (26)

$$g_i = \begin{cases} \frac{2}{\pi} \ln(\omega/\omega_o) & \text{for constant Q} \\ \cot \frac{\pi\nu}{2} \left[1-(\omega/\omega_o)^{-\nu}\right] & \text{for power law Q} \end{cases}$$

$$h_i = \begin{cases} 1 & \text{for constant Q} \\ (\omega/\omega_o)^{-\nu} & \text{for power law Q} \end{cases}$$

With the inversion at a reference frequency, the matrix equation (6) for Love waves is as given in Paper I. For Rayleigh waves, the matrix equation (7) becomes

$$\begin{pmatrix} \Delta c_1 \\ \Delta c_2 \end{pmatrix}_i = \begin{pmatrix} \frac{\partial c_1}{\partial \beta_1^o} & \frac{\partial c_1}{\partial \beta_2^o} & \frac{\partial c_1}{\partial \alpha_1^o} & \frac{\partial c_1}{\partial \alpha_2^o} & \frac{\partial c_1}{\partial \rho} \\ \frac{\partial c_2}{\partial \beta_1^o} & \frac{\partial c_2}{\partial \beta_2^o} & \frac{\partial c_2}{\partial \alpha_1^o} & \frac{\partial c_2}{\partial \alpha_2^o} & \frac{\partial c_2}{\partial \rho} \end{pmatrix}_{ij} \begin{pmatrix} \Delta\beta_1 \\ \Delta\beta_2 \\ \Delta\alpha_1 \\ \Delta\alpha_2 \\ \Delta\rho \end{pmatrix}_{\omega_o, j}$$

$$= \left[\left(\frac{\partial c_1}{\partial \beta_1}\right) \begin{pmatrix} 1 & g+\delta_1 h \\ -\delta_1 & h-g\delta_1 \end{pmatrix}, \left(\frac{\partial c_1}{\partial \alpha_1}\right) \begin{pmatrix} 1 & g+\delta_2 h \\ -\delta_2 & h-g\delta_2 \end{pmatrix}, \begin{pmatrix} \frac{\partial c_1}{\partial \rho} \\ \frac{\partial c_2}{\partial \rho} \end{pmatrix} \right]_{ij} \begin{pmatrix} \Delta\beta_1 \\ \Delta\beta_2 \\ \Delta\alpha_1 \\ \Delta\alpha_2 \\ \Delta\rho \end{pmatrix}_{\omega_o, j} \qquad \text{(A.9)}$$

where

$$\delta_1 = \frac{\partial c_1}{\partial \beta_2} \Big/ \frac{\partial c_1}{\partial \beta_1}$$

and

$$\delta_2 = \frac{\partial c_1}{\partial \alpha_2} \Big/ \frac{\partial c_1}{\partial \alpha_1} .$$

ACKNOWLEDGEMENTS

We thank Brian Mitchell for providing us with supplementary information on his Q measurements in the Pacific, Jeff Weissel for providing us with his recent results on the ages of marginal basins in the western Pacific, and Walt Silva for both a copy of his paper prior to publication and a critical review of this manuscript. This research was supported by the Advanced Research Projects Agency and monitored by the Air Force Office of Scientific Research under contracts F44620-71-C-0049 and F44620-75-C-0064. One of us (S.C.S.) was also supported by an Alfred P. Sloan Research Fellowship.

REFERENCES

Anderson, D.L. and C.B. Archambeau (1964). The anelasticity of the earth, J. Geophys. Res. 69, 2071-2084.

Anderson, D.L. and R.S. Hart (1976). Absorption and the low velocity zone, Nature 263, 397-398.

Anderson, D.L., H. Kanamori, R.S. Hart, and H.-P. Liu (1977). The earth as a seismic absorption band, Science 196, 1104-1106.

Andrade, E.N. daC. (1911). On the viscous flow in metals, and allied phenomena, Proc. Roy. Soc. Lond. A84, 1-12.

Archambeau, C.B., E.A. Flinn, and D.G. Lambert (1969). Fine structure of the upper mantle, J. Geophys. Res. 74, 5825-5865.

Azimi, Sh.A., A.Y. Kalinin, V.B. Kalinin and B.L. Pivovarov (1968). Impulse and transient characteristics of media with linear and quadratic absorption laws, Izv. Earth Phys., English Trans., No. 2, 88-93.

Biswas, N.N. and L. Knopoff (1970). Exact earth-flattening calculation for Love waves, Bull. Seism. Soc. Am. 60, 1123-1137.

Biswas, N.N. and L. Knopoff (1974). The structure of the upper mantle under the United States from the dispersion of Rayleigh waves, Geophys. J. Roy. Astron. Soc. 36, 515-539.

Bolt, B.A. and J. Dorman (1961). Phase and group velocities of Rayleigh waves in a spherical gravitating earth, J. Geophys. Res., 66, 2965-2981.

Carpenter, E.W. and D. Davies (1966). Frequency dependent seismic phase velocities, an attempted reconcilation between the Jeffreys/Bullen and the Gutenberg models of the upper mantle, Nature 212, 134-135.

Christensen, R.M. (1971) Theory of Viscoelasticity, Academic Press, New York.

Der, Z.A. and M. Landisman (1972). Theory for errors, resolution, and separation of unknown variables in inverse problems, with application to the mantle and the crust in southern Africa and Scandinavia, Geophys. J. Roy. Astron. Soc. 27, 137-178.

Der, Z.A. and T.W. McElfresh (1977). The relation between anelastic attenuation and regional amplitude anomalies of short-period P waves in North America, Bull. Seism. Soc. Am. 67, 1303-1317, 1977.

Forsyth, D.W. (1975). The early structural evolution and anisotropy of the oceanic upper mantle, Geophys. J. Roy. Astr. Soc. 43, 103-162.

Forsyth, D.W. (1977). The evolution of the upper mantle beneath mid-ocean ridges, Tectonophysics 38, 89-118.

Futterman, W.I. (1962). Dispersive body waves, J. Geophys. Res. 67, 5279-5291.

Hart, R.S., D.L. Anderson and H. Kanamori (1976). Shear velocity and density of an attenuating earth, Earth Planet. Sci. Lett. 32, 25-34.

Hart, R.S., D.L. Anderson, and H. Kanamori (1977). The effect of attenuation on gross earth models, J. Geophys. Res. 82, 1647-1654.

Haskell, N.A. (1953). The dispersion of surface waves on multiplelayered media, Bull. Seismol. Soc. Amer. 43, 17-34, 1953.

Jeffreys, H. (1958). A modification of Lomnitz Law of creep in rocks, Geophys. J. Roy. Astron. Soc. 1, 92-95.

Jeffreys, H. (1965). Damping of S waves, Nature 208, 675.

Jeffreys, H. (1975). Importance of damping in geophysics, Geophys. J. Roy. Astron. Soc. 40, 23-27.

Jeffreys, H. and S. Crampin (1960). Rock creep: a correction, Mon. Not. Roy. Astron. Soc. 121, 571-577.

Jordan, T.H. and S.A. Sipkin (1977). Estimation of the attenuation operator for multiple ScS waves, Geophys. Res. Lett. 4, 167-170.

Kanamori, H. and D.L. Anderson (1977). Importance of physical dirpersion in surface wave and free oscillation problems: review, Rev. Geophys. Space Phys. 15, 105-112.

Lamb, G.L., Jr. (1962). The attenuation of waves in a dispersive medium, J. Geophys. Res. 67, 5273-5277.

Lee, W.B. (1977). Simultaneous inversion of surface wave phase velocity and attenuation for continental and oceanic paths, Ph.D. thesis, M.I.T., Cambridge, MA, 274 pp.

Lee, W.B. and S.C. Solomon (1975). Inversion schemes for surface wave attenuation and Q in the crust and the mantle, Geophys. J. Roy. Astron. Soc. 43, 47-71.

Lee, W.B., and S.C. Solomon (1978). Simultaneous inversion of surface wave phase velocity and attenuation: Love waves in western North America, J. Geophys. Res., 83, 3389-3400.

Liu, H.-P., D.L. Anderson, and H. Kanamori (1976). Velocity dispersion due to anelasticity: implications for seismology and mantle composition, Geophys. J. Roy. Astron. Soc. 47, 41-58, 1976.

Lomnitz, C. (1957). Linear dissipation in solids, J. Appl. Phys. 57, 201-205.

McEvilly, T.V. (1964). Central United States crust-upper mantle structure from Love and Rayleigh wave phase velocity inversion, Bull. Seism. Soc. Am. 54, 1997-2015.

Mitchell, B.J. (1976). Anelasticity of the crust and upper mantle beneath the Pacific Ocean from the inversion of observed surface wave attenuation, Geophys. J. Roy. Astr. Soc. 46, 521-533.

Mitchell, B.J., L.W.B. Leite, Y.K. Yu, and R.B. Herrmann, (1976). Attenuation of Love and Rayleigh waves across the Pacific at periods between 15 and 110 seconds, Bull. Seism. Soc. Am., 66, 1189-1201.

Morse, P.M., and H. Feshbach (1953). Methods of Theoretical Physics, McGraw-Hill Book Co., New York, 1953.

North, R.G. and A.M. Dziewonski (1976). A note on Rayleigh-wave flattening corrections, Bull. Seism. Soc. Am., 66, 1873-1879.

Pitman, W.C., III, R.L. Larson, and E.M. Herron (1974). Magnetic lineations of the oceans (Map), Geol. Soc. of Amer., Boulder, CO.

Randall, M.J. (1976). Attenuative dispersion and frequency shifts of the earth's free oscillations, Phys. Earth Planet. Int. 12, P1-P4.

Schwab, F. and L. Knopoff (1971). Surface waves on multilayered anelastic media, Bull. Seism. Soc. Am. 61, 893-912, 1971.

Schwab, F. and L. Knopoff (1972). Fast surface wave and free mode computations, in Methods in Computational Physics, 11, B.A. Bolt, editor, Academic Press, New York, 87-180.

Sclater, J.G., D. Karig, L.A. Lawver, and K. Louden (1976). Heat flow, depth, and crustal thickness of the marginal basins of the south Philippine Sea, J. Geophys. Res., 81, 309-318.

Silva, W. (1978). Inversion of Love wave data for velocity and anelasticity using exact kernels, Geophys. J. Roy. Astron. Soc., in press.

Solomon, S.C. (1971). Seismic-wave attenuation and the state of the upper mantle, Ph.D. Thesis, M.I.T., Cambridge, MA, 321 pp.

Solomon, S.C. (1972a). Seismic-wave attenuation and partial melting in the upper mantle of North America, J. Geophys. Res., 77, 1483-1502.

Solomon, S.C. (1972b). On Q and seismic discrimination, Geophys. J. Roy. Astron. Soc. 31, 163-177.

Solomon, S.C., R.W. Ward, and M.N. Toksöz (1970). Earthquake and explosion magnitudes: the effect of lateral variation of seismic attenuation, Copies of papers presented at Woods Hole Conference on Seismic Discrimination, Vol. 1, Advanced Research Projects Agency, July 20-23.

Strick, E. (1967). The determination of a dynamic viscosity and transient creep curve from wave propagation measurements, Geophys. J. Roy. Astron. Soc. 13, 197-218.

Tryggvason, E. (1965). Dissipation of Rayleigh wave energy, J. Geophys. Res. 70, 1449-1455.

Tsai, Y.B., and K. Aki (1969). Simultaneous determination of the seismic moment and attenuation of seismic surface waves, Bull. Seism. Soc. Am., 59, 275-287.

Watts, A.B., J.K. Weissel, and F.J. Davey (1977). Tectonic evolution of the south Fiji marginal basin, in Island Arcs, Deep Sea Trenches and Back-Arc Basins, Maurice Ewing Series 1, ed. by M. Talwani and W.C. Pitman III,

Amer. Geophys. Un., Washington, D.C., 419-427.

Weissel, J.K. (1977). Evolution of the Lau basin by the growth of small plates, in Island Arcs, Deep Sea Trenches and Back-Arc Basins, Maurice Ewing Series 1, ed. by M. Talwani and W.C. Pitman III, Amer. Geophys. Un., Washington, D.C., 429-436.

Weissel, J.K., A.B. Watts, A. Lapouille, G. Karner, and D. Jongsma (1977). Preliminary results from recent geophysical investigations in marginal basins of Melanesia (abstract), EOS Trans. Amer. Geophys. Un. 58, 504.

Zener, C.M. (1948). Elasticity and Anelasticity of Metals, University of Chicago Press, IL, 170 pp.

Table 1. Fraction of great circle paths in each age group for the 26 April 1973 Pacific event

Path	Distance (°)	Percentage
0-5 m.y. ocean	19.99	1.54
5-10 "	33.96	2.61
10-20 "	98.86	7.59
20-38 "	26.06	2.00
38-53 "	205.87	15.81
53-65 "	137.22	10.54
65-83 "	23.00	1.77
83-100 "	303.73	22.33
100-135 "	179.77	13.81
135-190 "	150.17	11.53
> 190 "	5.86	0.45
North American* continent	32.57	8.27
South American continent	9.83	0.76
Total	1302.04	100

*Continental paths in southeast Asia are included in this group.

Table 2. Starting model for inversion of combined Love and Rayleigh phase velocity and attenuation in western North America (case $\nu = 0$)

Depth, km	β, km/sec	α, km/sec	ρ, g/cm^3	100/Q
0-2*	1.72	4.00	2.21	.32
2-13	3.58	6.00	2.80	.32
13-21	3.58	6.20	2.80	.32
21-45	3.96	6.50	3.25	.13
45-64	4.54	7.619	3.40	.13
64-84	4.54	7.615	3.40	.13
84-94	4.48	7.615	3.45	5.93
94-128	4.49	7.619	3.45	5.93
128-160	4.49	7.622	3.45	5.93
160-180	5.27	7.90	3.50	2.96
180-220	5.27	8.23	3.50	2.96
220-260	5.27	8.25	3.50	2.96
260-300	5.27	8.27	3.50	2.96
300-350	5.27	8.43	3.50	2.96
Halfspace*	5.27	8.53	3.90	2.96

*Parameters fixed during inversion for these layers.

Table 3. Envelopes of shear velocity and shear attenuation at 1 Hz and of density from the simultaneous inversion of Love and Rayleigh wave phase velocity and attenuation in western North America.

Layer no.	Depth (km)	minimum β, km/sec S31W	S32W	S33W	maximum β, km/sec S31W	S32W	S33W
2	2-21	3.527	3.529	3.533	3.492	3.621	3.637
3	21-45	3.897	3.886	3.812	4.012	4.052	4.029
4	45-84	4.382	4.259	4.293	4.583	4.549	4.690
5	84-160	4.105	4.012	3.823	4.463	4.412	4.263
6	160-350	4.782	4.750	4.702	5.500*	5.500*	5.500*

Layer no.	Depth (km)	minimum $100/Q_\beta$ S31W	S32W	S33W	maximum $100/Q_\beta$ S31W	S32W	S33W
2	2-21	0.274	0.148	0.051	0.490	0.282	0.118
3	21-45	0.059	0.0	0.0	0.250	0.149	0.105
4	45-84	0.0	0.0	0.0	0.447	0.137	0.087
5	84-160	4.200	2.000	0.453	5.330	2.337	0.783
6	160-350	1.350	0.119	0.084	3.640	0.782	0.860

Layer no.	Depth (km)	minimum ρ, g/cm^3 S31W	S32W	S33W	maximum ρ, g/cm^3 S31W	S32W	S33W
2	2-21	2.807	2.846	2.850	2.90*	2.90*	2.90*
3	21-45	3.070	3.042	3.000*	3.30*	3.30*	3.30*
4	45-84	3.200*	3.200*	3.200*	3.434	3.50*	3.50*
5	84-160	3.200*	3.200*	3.200*	3.491	3.441	3.50*

*A priori bounds not well resolved by the inversion

Table 4. Starting model for inversion of Love and Rayleigh wave phase velocity and attenuation in east-central North America (case $\nu = 0$)

Depth, km	β, km/sec	α, km/sec	ρ, g/cm^3	$100/Q_\beta$
0-11	3.50	6.10	2.9	0.1
11-20	3.68	6.20	2.9	0.1
20-38	3.94	6.40	2.9	0.1
38-62	4.75	8.15	3.3	0.1
62-102	4.61	8.20	3.3	0.1
102-135	4.45	8.20	3.4	0.1
135-350	4.45	8.20	3.4	2.3
Halfspace*	4.80	8.70	3.6	2.3

*Parameters fixed during inversion for this layer.

Table 5. Envelopes of shear velocity and shear attenuation at 1 Hz and density from the simultaneous inversion of Love and Rayleigh wave phase velocity and attenuation in east-central North America

Layer no.	Depth (km)	Minimum β, km/sec S31E	Minimum β, km/sec S32E	Maximum β, km/sec S31E	Maximum β, km/sec S32E
1	0-38	3.684	3.659	3.692	3.666
2	38-82	4.557	4.478	4.594	4.513
3	82-134	5.092	4.719	5.321	4.890
4	134-350	5.200	5.147	5.500*	5.500*

Layer no.	Depth (km)	Minimum $100/Q_\beta$ S31E	Minimum $100/Q_\beta$ S32E	Maximum $100/Q_\beta$ S31E	Maximum $100/Q_\beta$ S32E
1	0-38	0.165	0.037	0.263	0.055
2	38-82	0.0	0.0	0.222	0.048
3	82-134	3.056	0.241	5.630	0.831
4	134-350	0.182	0.036	3.846	0.364

Layer no.	Depth (km)	Minimum ρ, g/cm^3, S31E	Minimum ρ, g/cm^3, S32E	Maximum ρ, g/cm^3 S31E	Maximum ρ, g/cm^3 S32E
1	0-38	2.896	2.895	2.900*	2.900*
2	38-82	3.200*	3.000*	3.241	3.010
3	82-134	3.200*	3.200*	3.327	3.220
4	134-350	3.600*	3.600*	3.800*	3.800*

*A priori bounds not well resolved by the inversion.

Table 6. Starting model for the inversion of Rayleigh wave phase velocity and attenuation in central Pacific

Depth, km	β, km/sec	α, km/sec	ρ, g/cm^3	$100/Q_\beta$
0-5*	0.0	1.52	1.03	0.0
5-5.2*	1.0	1.70	2.20	0.80
5.2-12*	3.76	6.53	3.00	0.60
12-47	4.60	8.17	3.34	0.60
47-67	4.35	7.70	3.40	0.50
67-107	4.35	7.70	3.44	1.00
107-147	4.35	7.70	3.44	1.20
147-227	4.35	7.70	3.44	1.00
227-302	4.60	8.49	3.50	0.60
302-402	4.80	8.81	3.50	0.40
Halfspace*	5.00	9.00	3.76	0.40

*Parameters held fixed during inversion for these layers.

Table 7. Envelopes of shear velocity and shear attenuation at 1 Hz in the Pacific

Layer no.	Depth (km)	Minimum β	Maximum β
4	12-57	4.542	4.571
5	57-107	4.195	4.350
6	107-227	4.212	4.516
7	227-402	4.50*	5.00*

Layer no.	Depth (km)	Minimum $100/Q_\beta$	Maximum $100/Q_\beta$
4	12-57	0.413	0.440
5	57-107	1.295	1.742
6	107-227	0.900	1.695
7	227-402	0.404	2.000

*A priori bounds not well resolved by the inversion.

Figure Captions

Fig. 1. Pacific area map showing paths between the April 26, 1973 earthquake and stations (ALQ, ANP, ARE, BAG, BOG, CHG, COL, COR, DAV, HKC, JCT, LPB, NIL, RAR, RIV, SNG, TAU, TUC, WEL) used in the Q^{-1} measurements of Mitchell et al. (1976). Azimuthal equidistant projection about 0°N, 180°E.

Fig. 2. Rayleigh wave phase velocity for the central Pacific. Circles with error bars are calculated as a weighted average of 'pure path' velocities (Forsyth, 1975, 1977), including measurement uncertainties, using the magnetic anomaly map of Pitman et al. (1974). The solid lines are the envelope associated with extremal earth models for inversion S21P. The dashed line is the predicted dispersion for the model shown as dashed in Figure 17.

Fig. 3. Selected partial derivatives of the real part of Rayleigh wave phase velocity with respect to the imaginary part of shear velocity ($\partial c_1^R/\partial \beta_2$, solid lines) and to the real part of shear wave velocity ($\partial c_1^R/\partial \beta_1$, dashed lines) per unit layer thickness for the initial model in Table 2. The partials shown are for frequency-independent Q^{-1} at the frequency indicated; for frequency-dependent Q^{-1} relations, the partial derivatives have a similar structure.

Discontinuities in the partials occur at discontinuities in the initial model.

Fig. 4. Resolving kernels for (a) shear velocity and (b) shear attenuation at selected depths (arrows) at the reference frequency 1 Hz, using both Love and Rayleigh wave data in western North America for the case of Q independent of frequency. Model standard deviations are shown at the right.

Fig. 5. Envelopes of shear velocity and shear attenuation, at a frequency of 1 Hz, and density for models S31W, S32W and S33W. Solid lines represent envelopes of S31W ($\nu = 0$), short-dashed lines are for S32W ($\nu = 1/5$) and long-dashed lines are for S33W ($\nu = 1/2$).

Fig. 6. Love wave phase velocity, western North America. Observations are shown by circles; vertical bars represent standard deviations. The envelope (solid lines) is associated with the extreme earth model bounds from inversion S31W. Open circles are incompatible data for this inversion.

Fig. 7. Rayleigh wave phase velocity, western North America. Observations are shown by circles; vertical bars represent standard deviations. The envelope (solid lines) is associated with the extreme earth model bounds from inversion S31W. Open circles are incompatible data for this inversion.

Fig. 8. Love wave attenuation, western North America. Circles are observations; vertical bars represent standard deviations. The solid lines represent the envelope associated with extremal earth models for inversion S31W.

Fig. 9. Rayleigh wave attenuation, western North America. Circles are observations; vertical bars represent standard deviations. The solid lines represent the envelope associated with extremal earth models for inversion S31W. Open circles are incompatible data for this inversion.

Fig. 10. Resolving kernels for (a) shear velocity and (b) shear attenuation at selected depths (arrows) at the reference frequency 1 Hz, using both Love and Rayleigh wave phase velocity and attenuation in east-central North America for the case of Q independent of frequency. Model standard deviations are shown at the right.

Fig. 11. Envelopes of shear velocity and shear attenuation, at a frequency of 1 Hz, and density for models S31E and S32E. Solid lines represent envelopes of S31E ($\nu = 0$), and dashed lines are for S32E ($\nu = 1/2$).

Fig. 12. Love wave phase velocity, east-central North America. Observations are shown by circles; vertical bars represent standard deviations. The envelope is associated with the extreme earth model bounds from inversion S31E. Open circles are incompatible data for this inversion.

Fig. 13. Rayleigh wave phase velocity, east-central North America. Observations are shown by circles; vertical bars represent standard deviations. The envelope is associated with the extreme earth model bounds from inversion S31E. Open circles are incompatible data for this inversion.

Fig. 14. Love wave attenuation, east-central North America. Circles are observations; vertical bars represent standard deviations. The solid lines represent the envelopes associated with extremal earth models for inversion S31E. Open circles are incompatible data for this inversion.

Fig. 15. Rayleigh wave attenuation, east-central North America. Circles are observations; vertical bars represent standard deviations. The solid lines represent the envelope associated with extremal earth models for inversion S31E.

Fig. 16. Resolving kernels for (a) shear velocity and (b) shear attenuation at selected depths (arrows), using Rayleigh wave data in the central Pacific for the case of Q independent of frequency. Model standard deviations are shown at the right.

Fig. 17. Envelopes of shear velocity (at 1 Hz) and shear attenuation for the central Pacific, model S21P (Q^{-1} independent of frequency). The dashed lines show the average of the models making up the envelopes.

Fig. 18. Rayleigh wave attenuation, central Pacific. Circles are observations; vertical bars represent standard deviations. The solid lines represent the envelope associated with extremal earth models for inversion S21P. Open circles are incompatible data for this inversion. The dashed line is Q_R^{-1} predicted for the model shown as dashed in Figure 17.

Figure 1

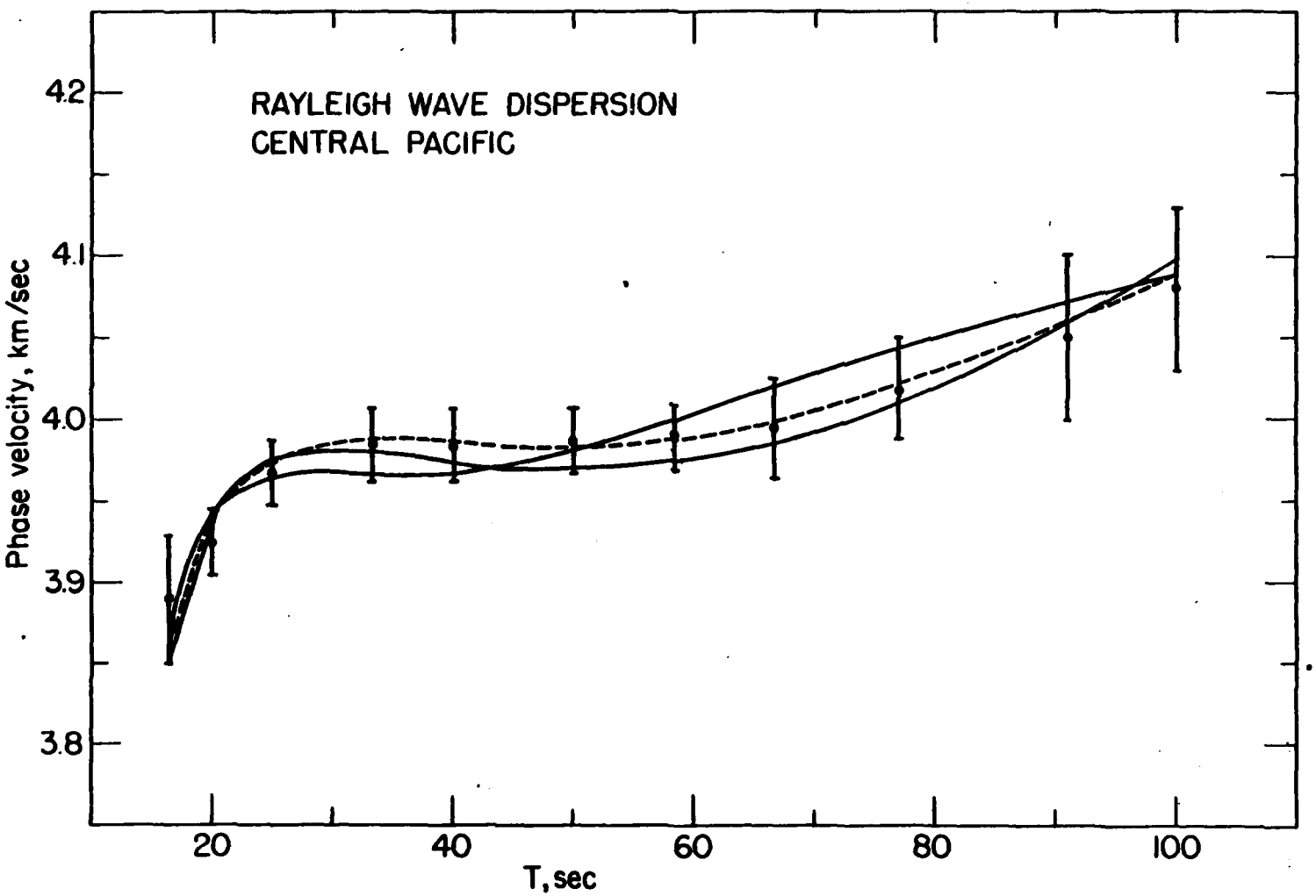
RAYLEIGH WAVE DISPERSION
CENTRAL PACIFIC
Phase velocity, km/sec
4.2
4.1
4.0
3.9
3.8
20
40
60
80
100
T, sec

Figure 2

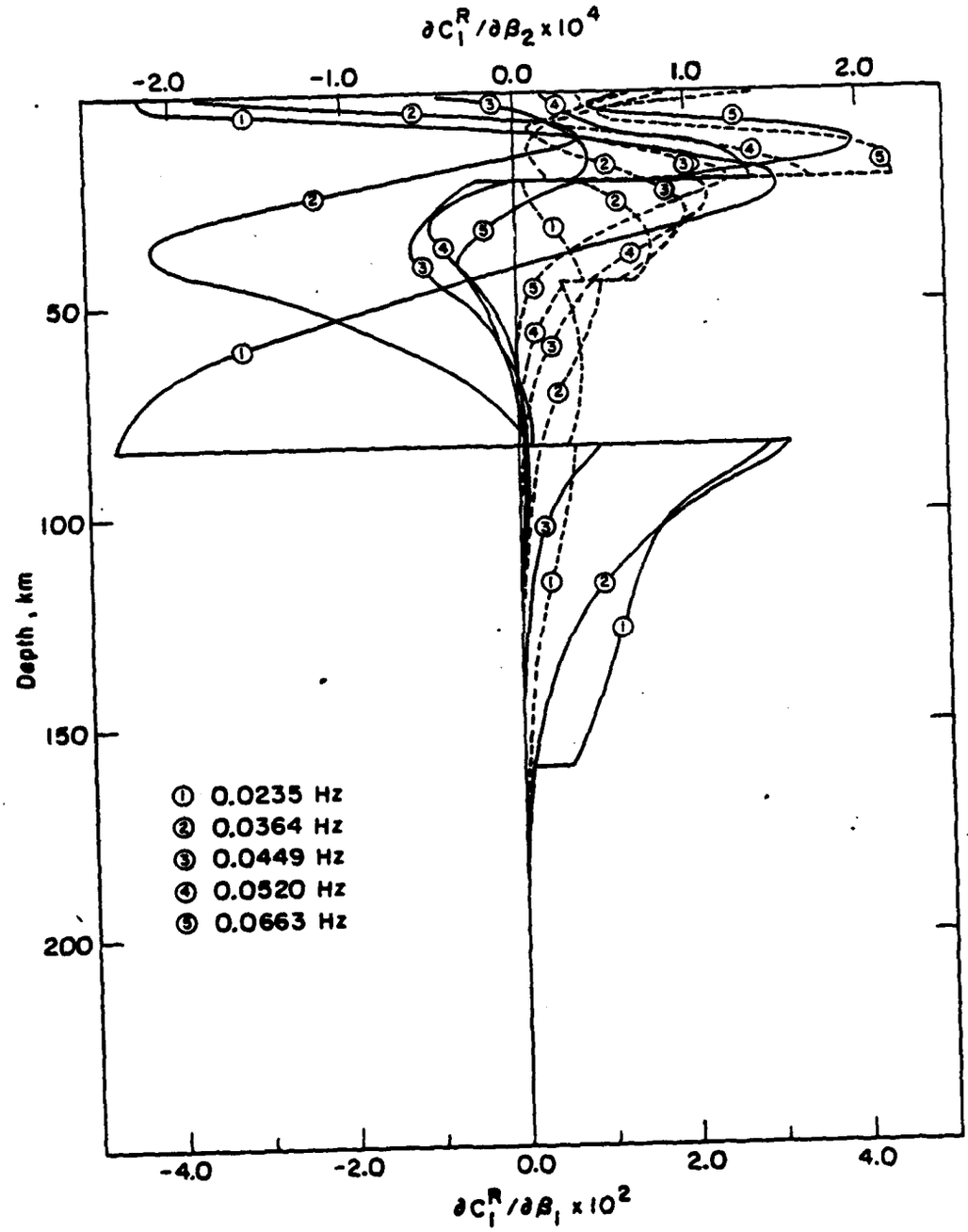
$\partial C_1^R/\partial\beta_2 \times 10^4$
-2.0
-1.0
0.0
1.0
2.0
50
100
150
200
Depth, km
① 0.0235 Hz
② 0.0364 Hz
③ 0.0449 Hz
④ 0.0520 Hz
⑤ 0.0663 Hz
-4.0
-2.0
0.0
2.0
4.0
$\partial C_1^R/\partial\beta_1 \times 10^2$

Figure 3

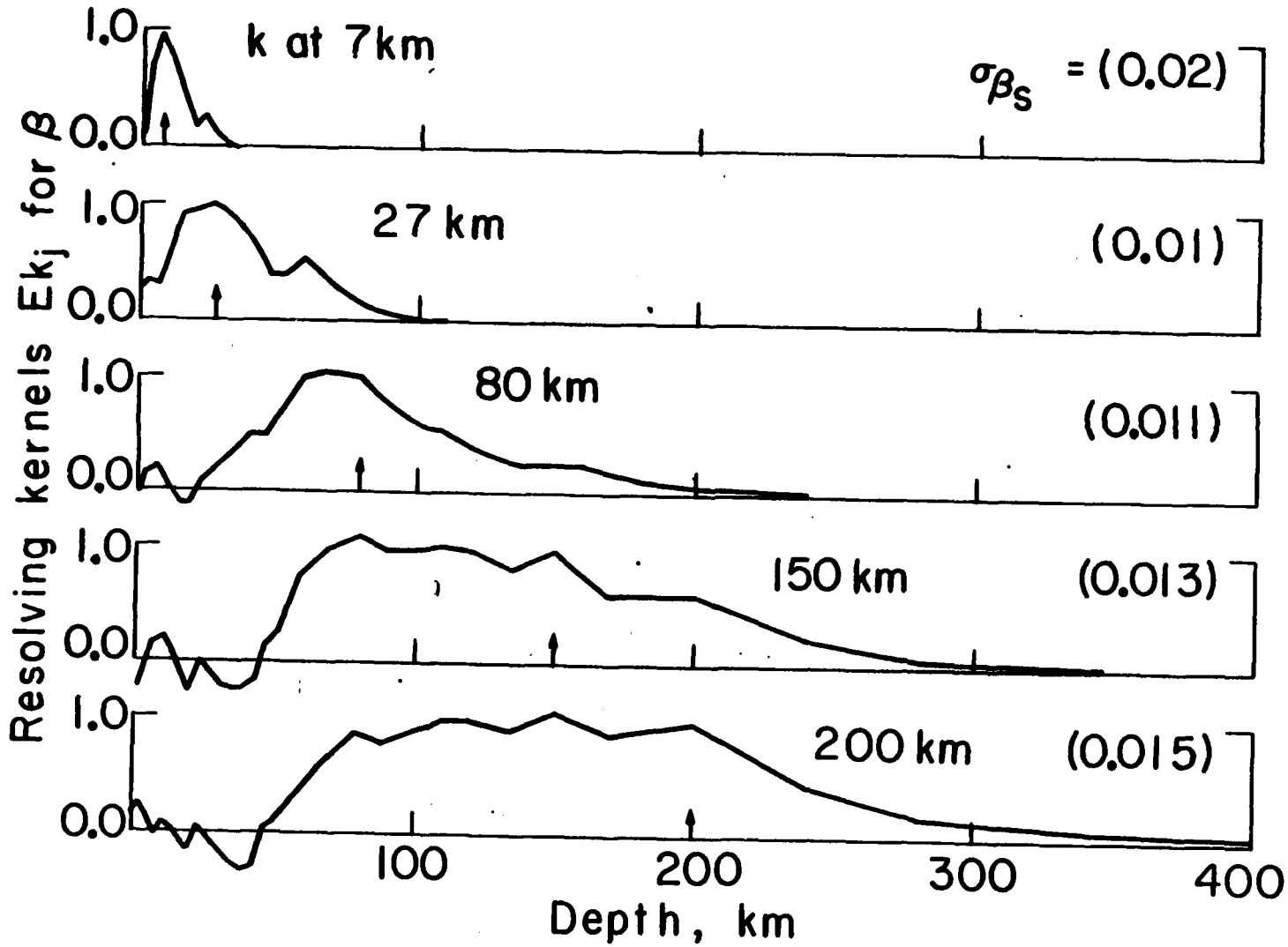
1.0
0.0
k at 7km
σ_{β_S} = (0.02)
27 km
(0.01)
80 km
(0.011)
150 km
(0.013)
200 km
(0.015)
Resolving kernels E_{kj} for β
100
200
300
400
Depth, km

Figure 4 a

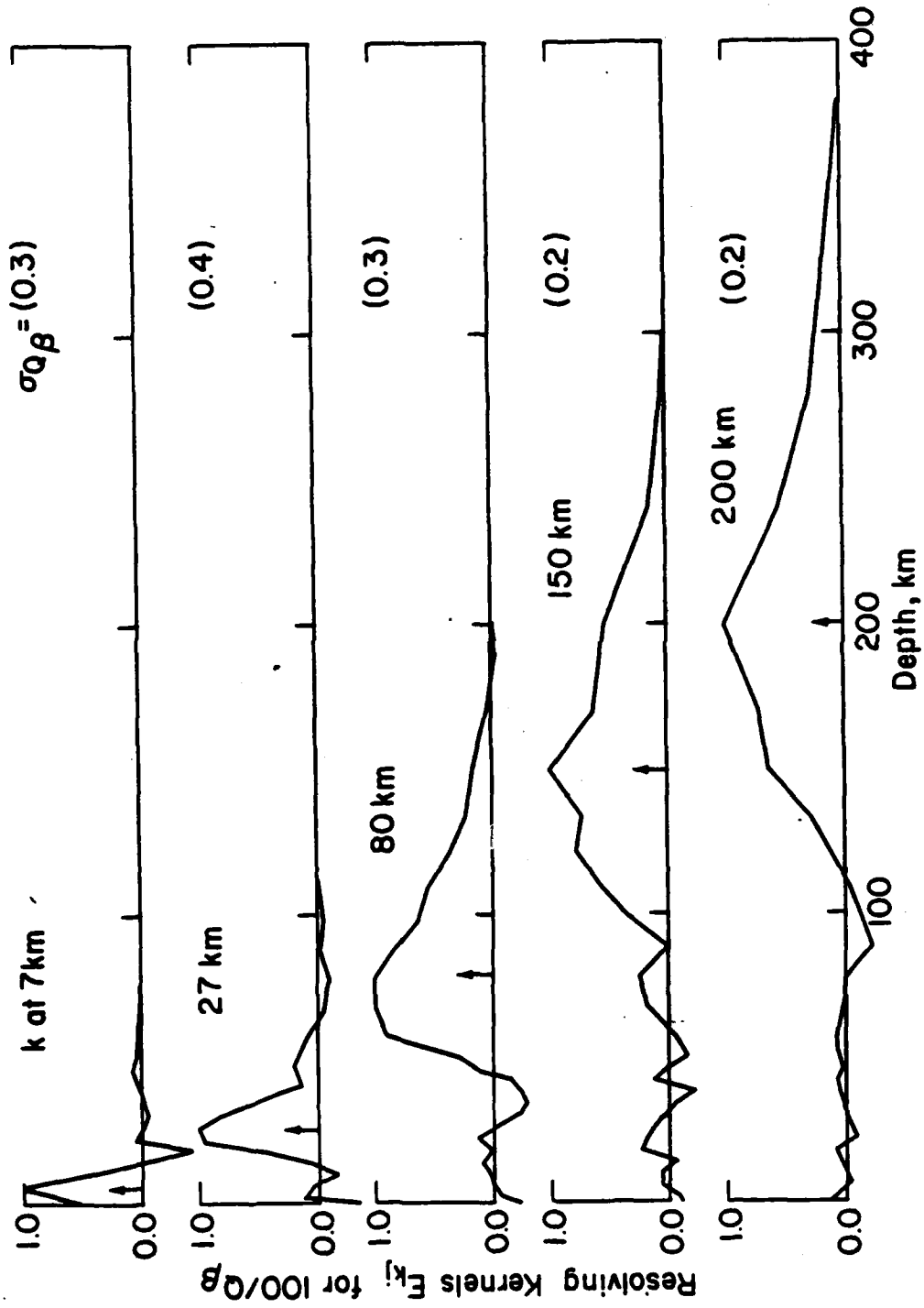
Resolving Kernels E_{kj} for $100/Q_\beta$
k at 7km
27 km
80 km
150 km
200 km
σ_{Q_β}=(0.3)
(0.4)
(0.3)
(0.2)
(0.2)
1.0
0.0
100
200
300
400
Depth, km

Figure 4 b

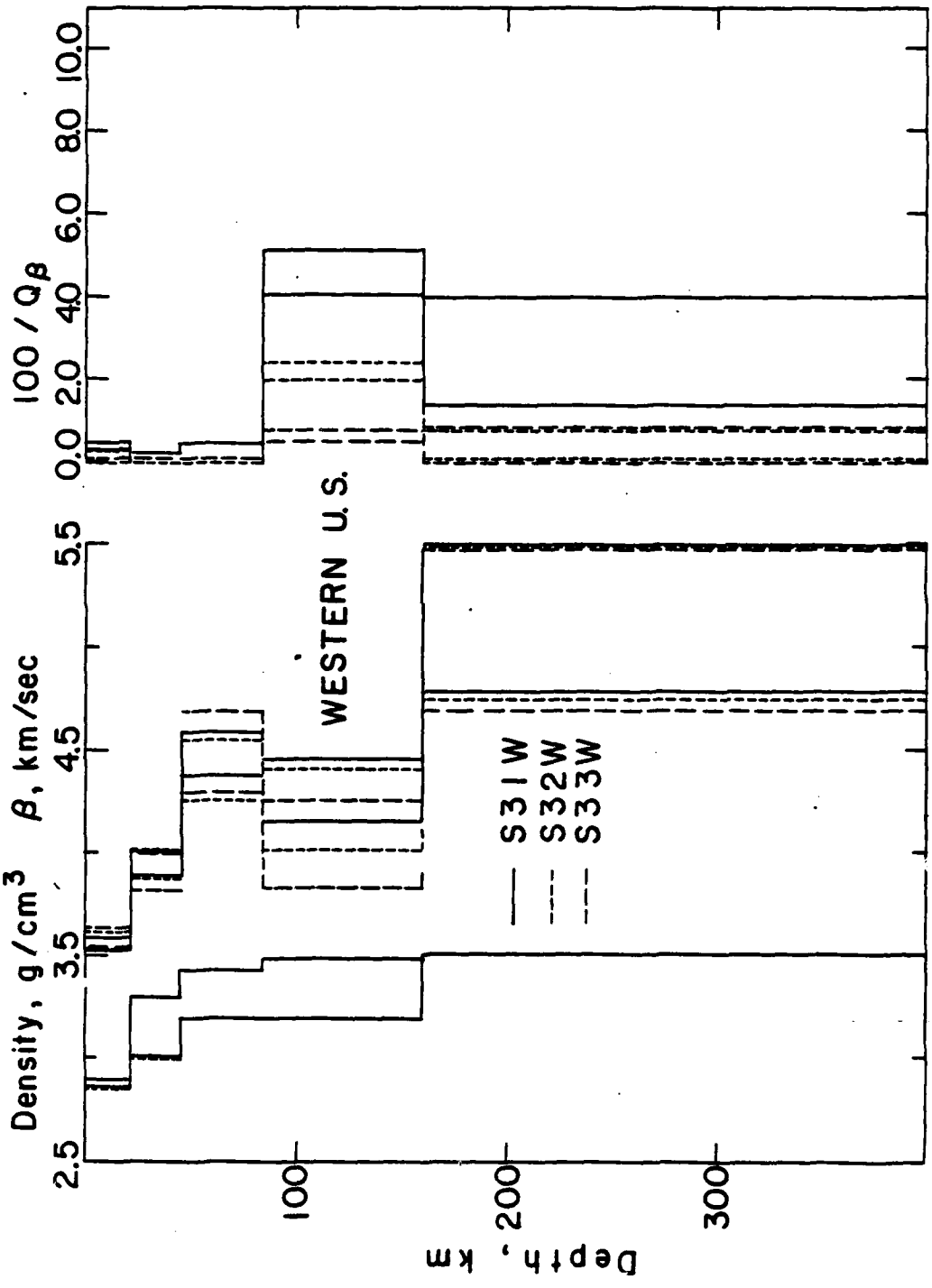
100 / Qβ
0.0
2.0
4.0
6.0
8.0
10.0
WESTERN U.S.
S31W
S32W
S33W
Density, g/cm3
β, km/sec
2.5
3.5
4.5
5.5
100
200
300
Depth, km

Figure 5

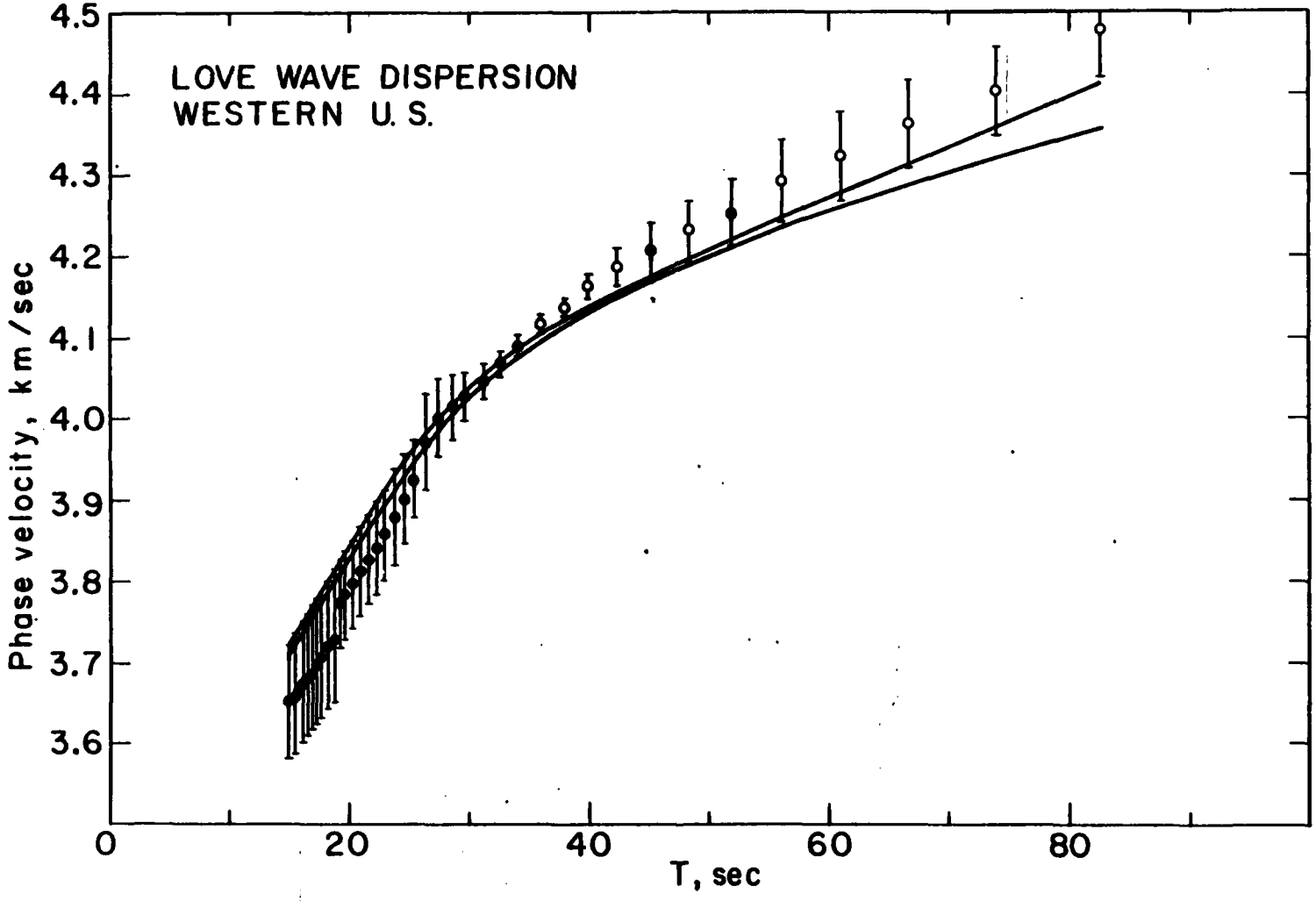
LOVE WAVE DISPERSION
WESTERN U. S.
Phase velocity, km/sec
4.5
4.4
4.3
4.2
4.1
4.0
3.9
3.8
3.7
3.6
0
20
40
60
80
T, sec

Figure 6

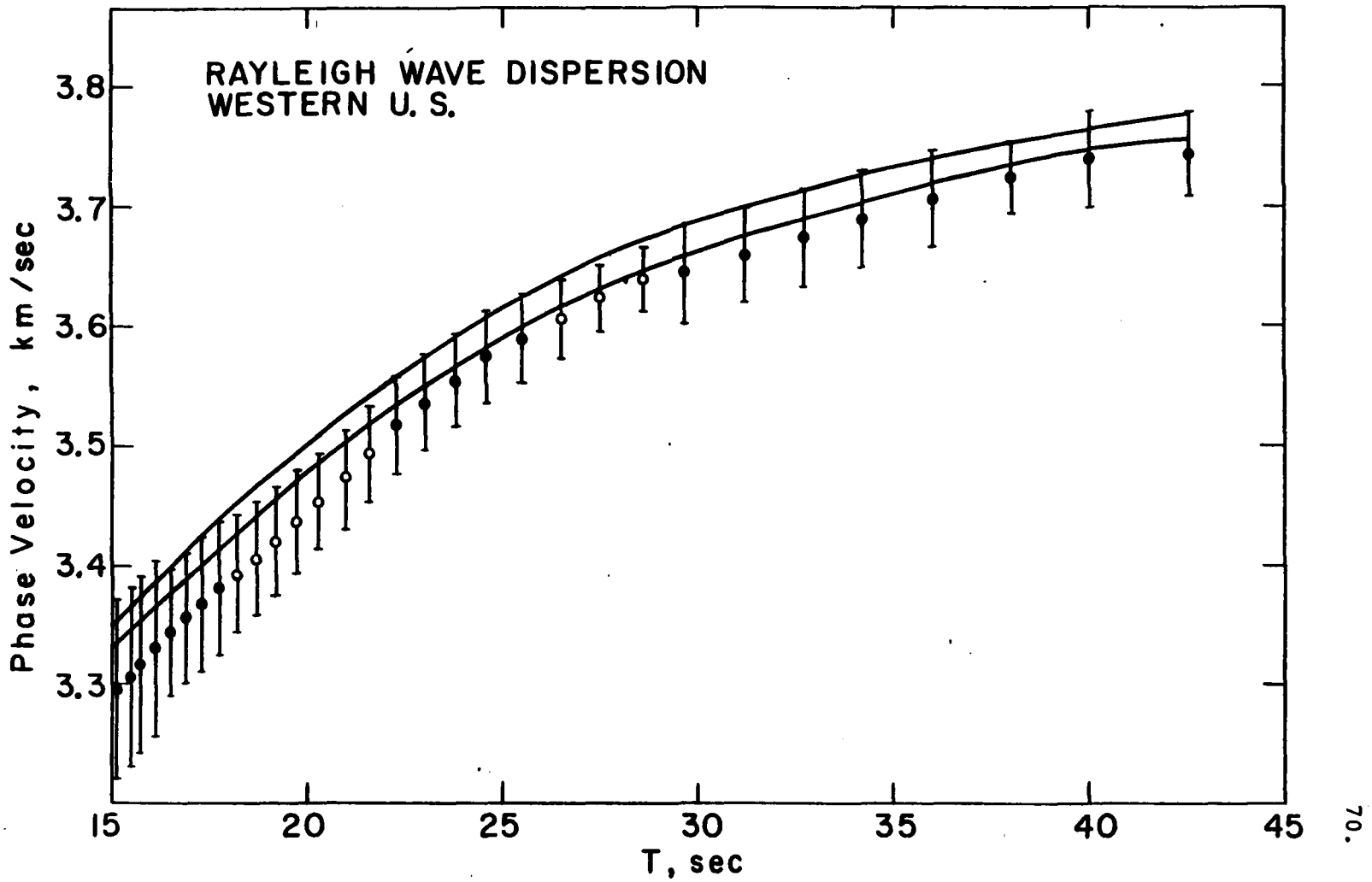
RAYLEIGH WAVE DISPERSION
WESTERN U. S.
Phase Velocity, km/sec
3.8
3.7
3.6
3.5
3.4
3.3
15
20
25
30
35
40
45
T, sec

Figure 7

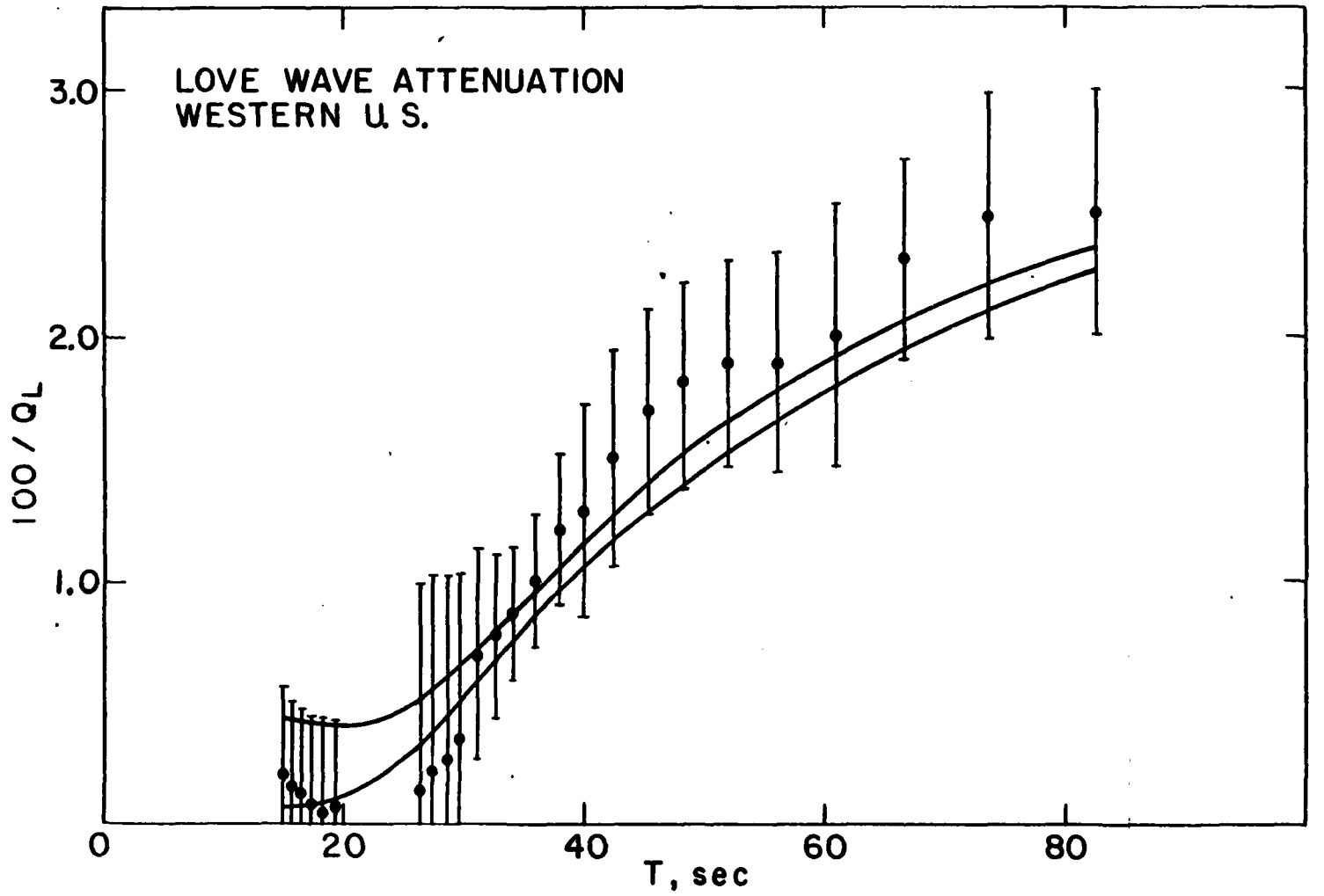
LOVE WAVE ATTENUATION
WESTERN U. S.
3.0
2.0
1.0
100 / Q_L
0
20
40
60
80
T, sec

Figure 8

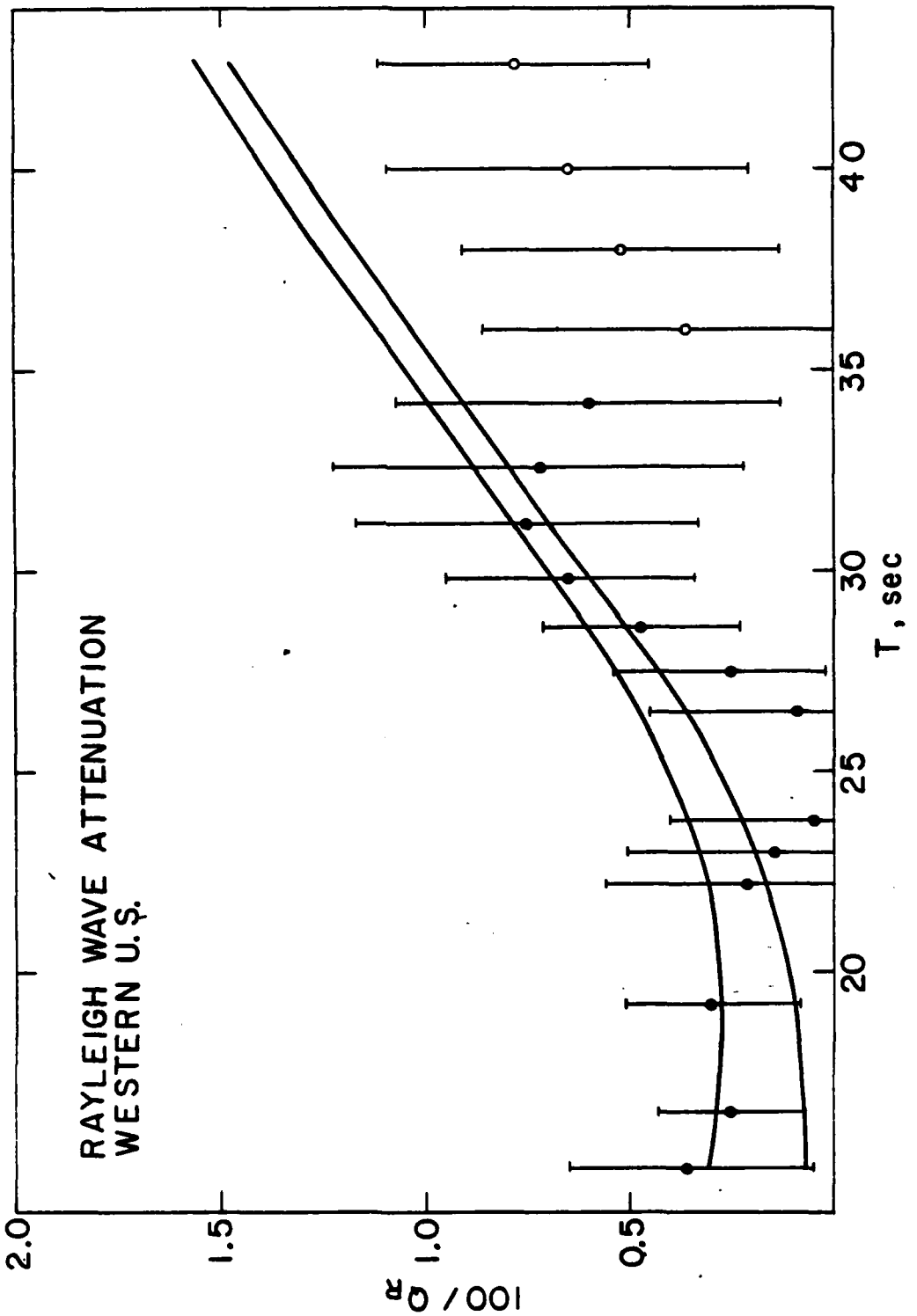
RAYLEIGH WAVE ATTENUATION
WESTERN U.S.
100 / Q_R
2.0
1.5
1.0
0.5
20
25
30
35
40
T, sec

Figure 9

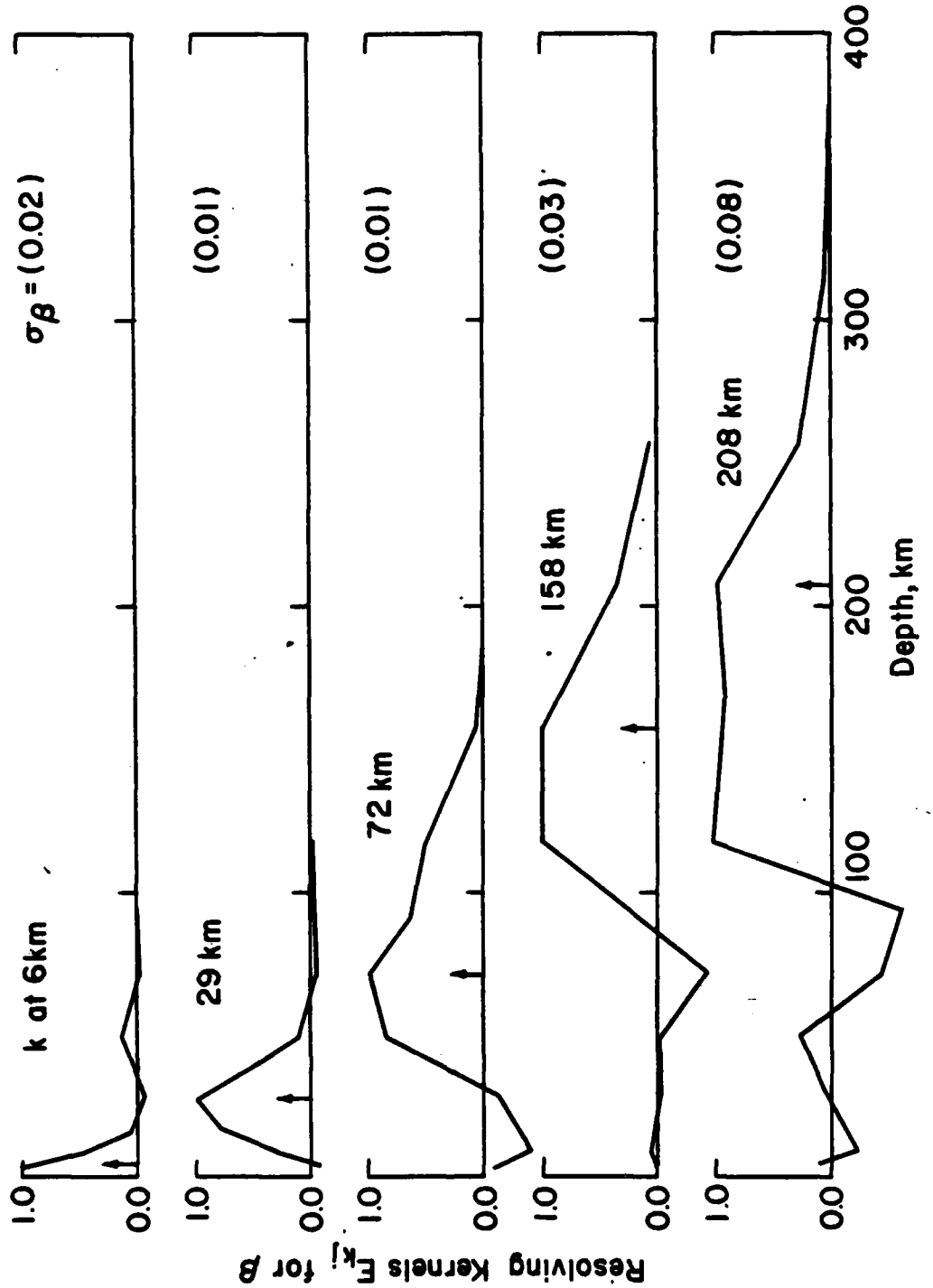
Resolving Kernels E_{kj} for β
1.0
0.0
k at 6km
29 km
72 km
158 km
208 km
σ_β = (0.02)
(0.01)
(0.01)
(0.03)
(0.08)
100
200
300
400
Depth, km

Figure 10a

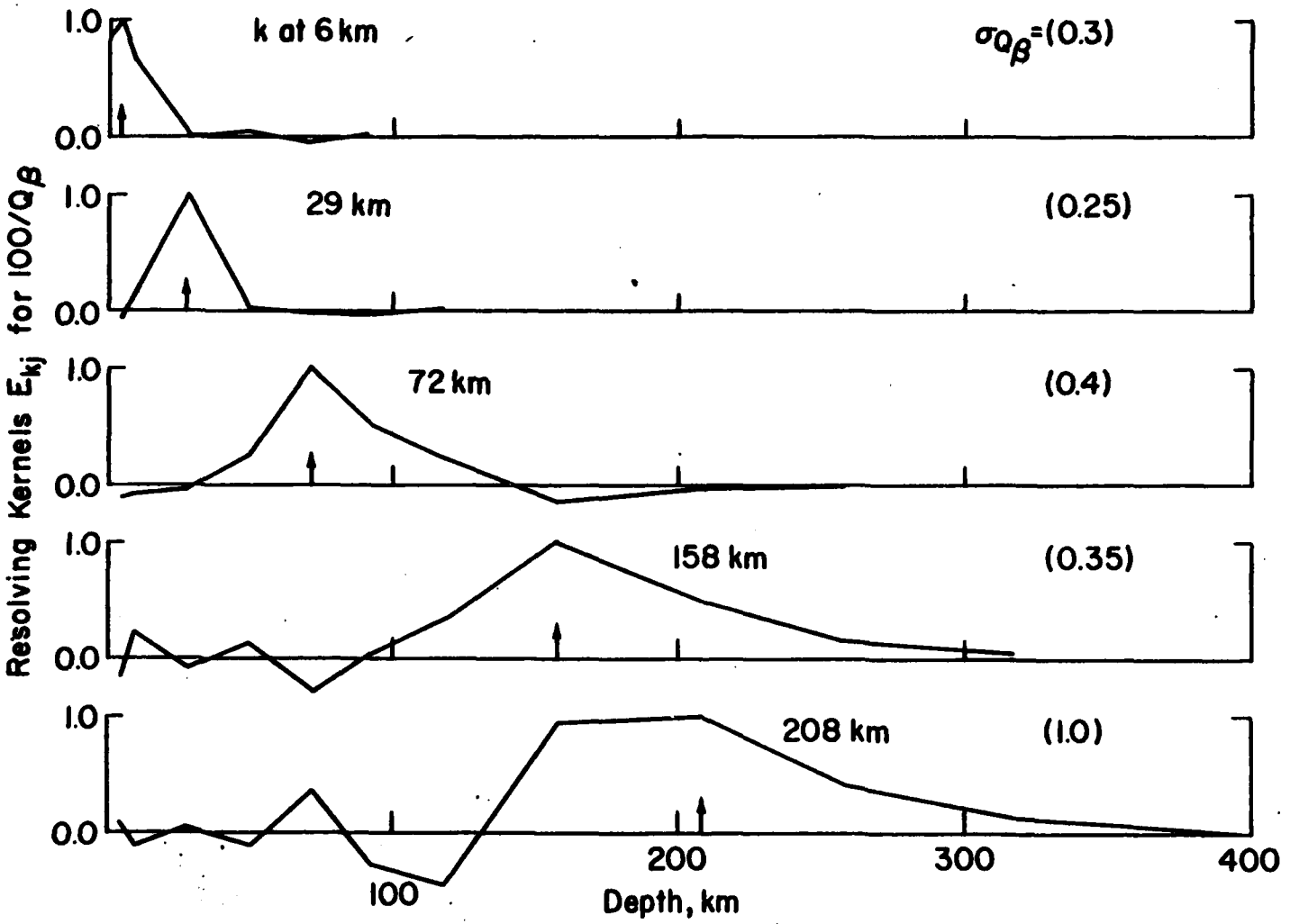
1.0
0.0
k at 6 km
$\sigma_{Q\beta}$=(0.3)
29 km
(0.25)
72 km
(0.4)
158 km
(0.35)
208 km
(1.0)
Resolving Kernels E_{kj} for $100/Q_\beta$
100
200
300
400
Depth, km

Figure 10b

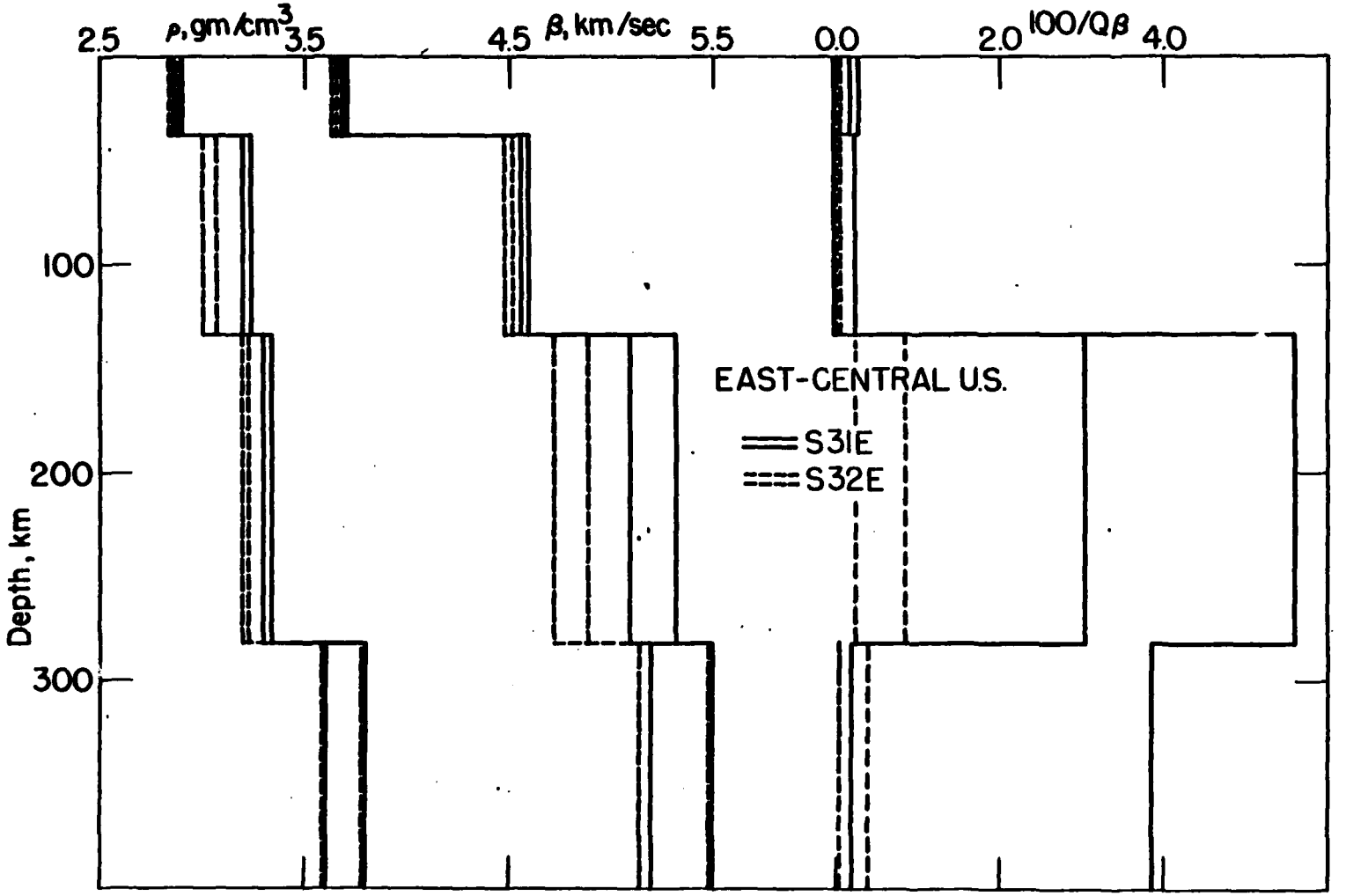
2.5
ρ, gm/cm3
3.5
4.5
β, km/sec
5.5
0.0
2.0
100/Qβ
4.0
100
200
300
Depth, km
EAST-CENTRAL U.S.
S31E
S32E

Figure 11

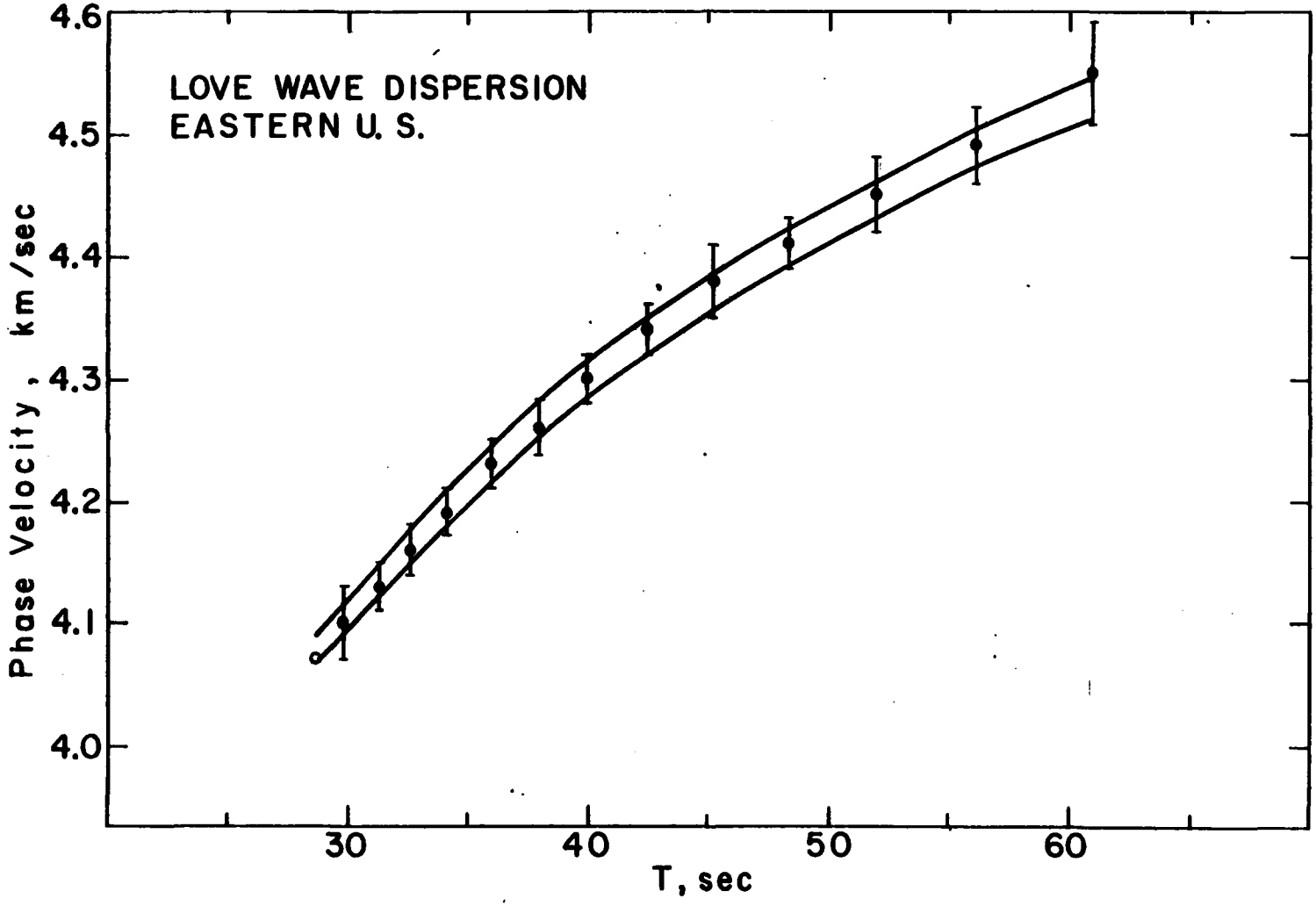
LOVE WAVE DISPERSION
EASTERN U. S.
Phase Velocity, km/sec
4.6
4.5
4.4
4.3
4.2
4.1
4.0
30
40
50
60
T, sec

Figure 12

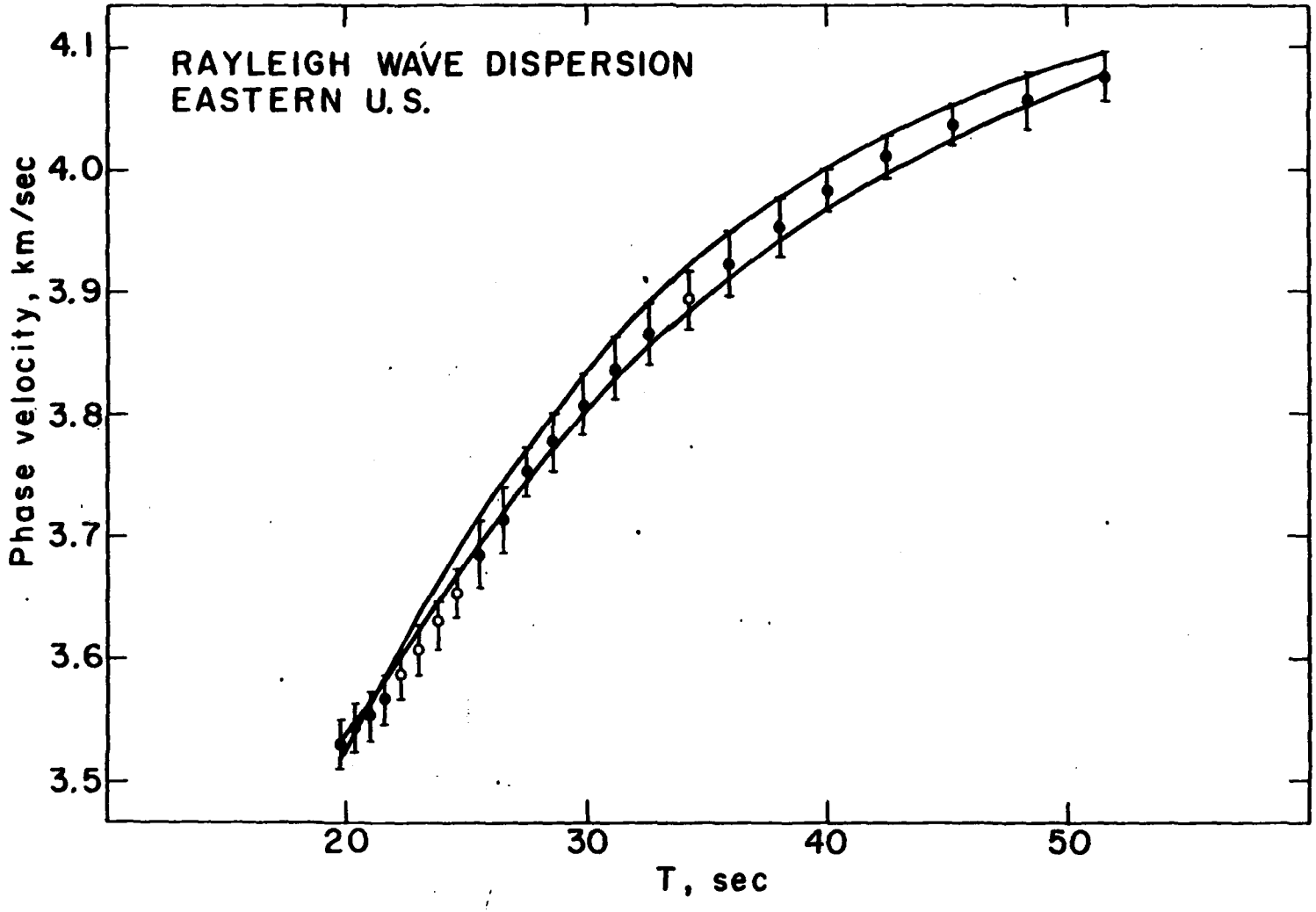
RAYLEIGH WAVE DISPERSION
EASTERN U.S.
Phase velocity, km/sec
4.1
4.0
3.9
3.8
3.7
3.6
3.5
20
30
40
50
T, sec

Figure 13

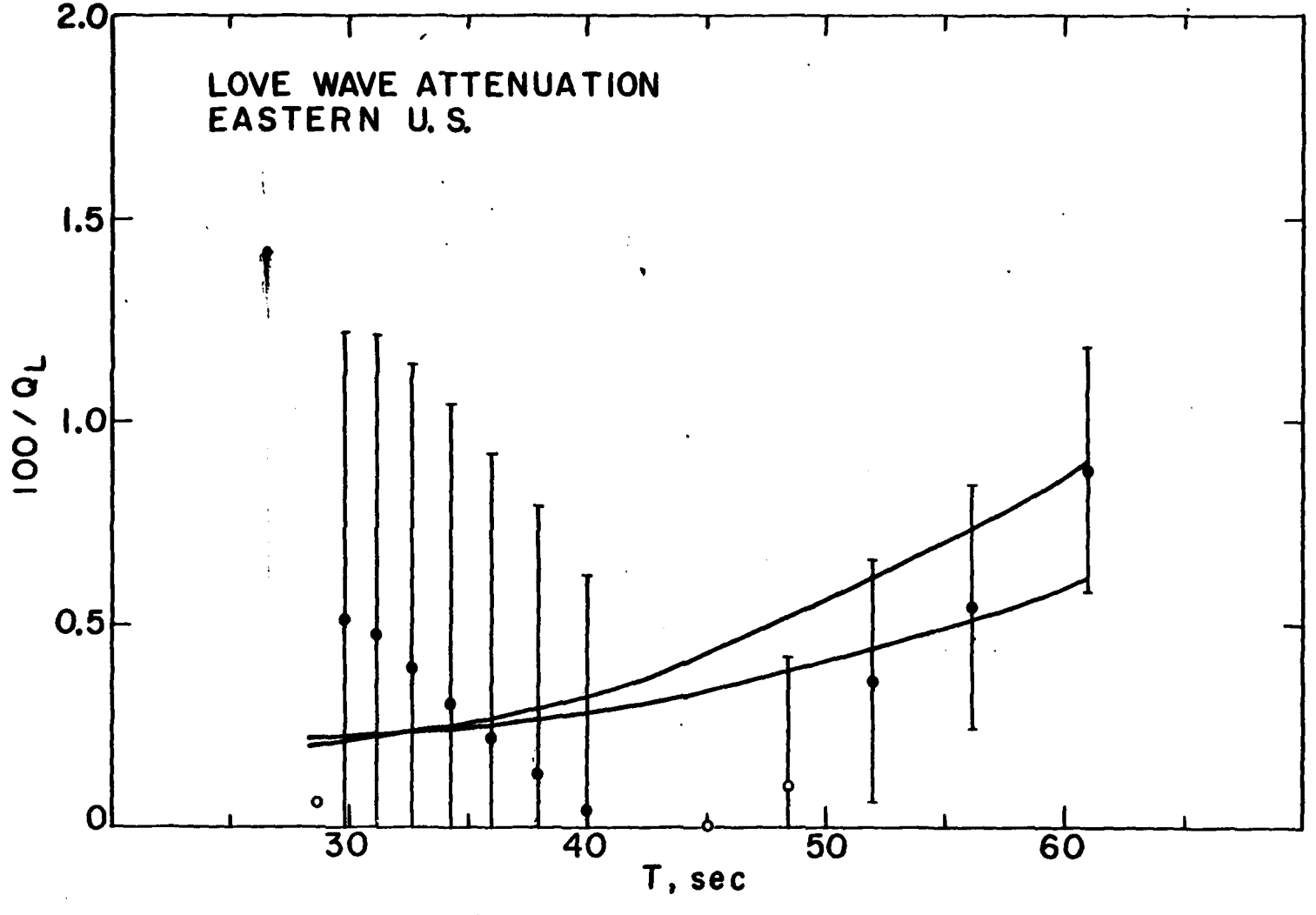
LOVE WAVE ATTENUATION
EASTERN U. S.
2.0
1.5
1.0
0.5
0
100 / Q_L
30
40
50
60
T, sec

Figure 14

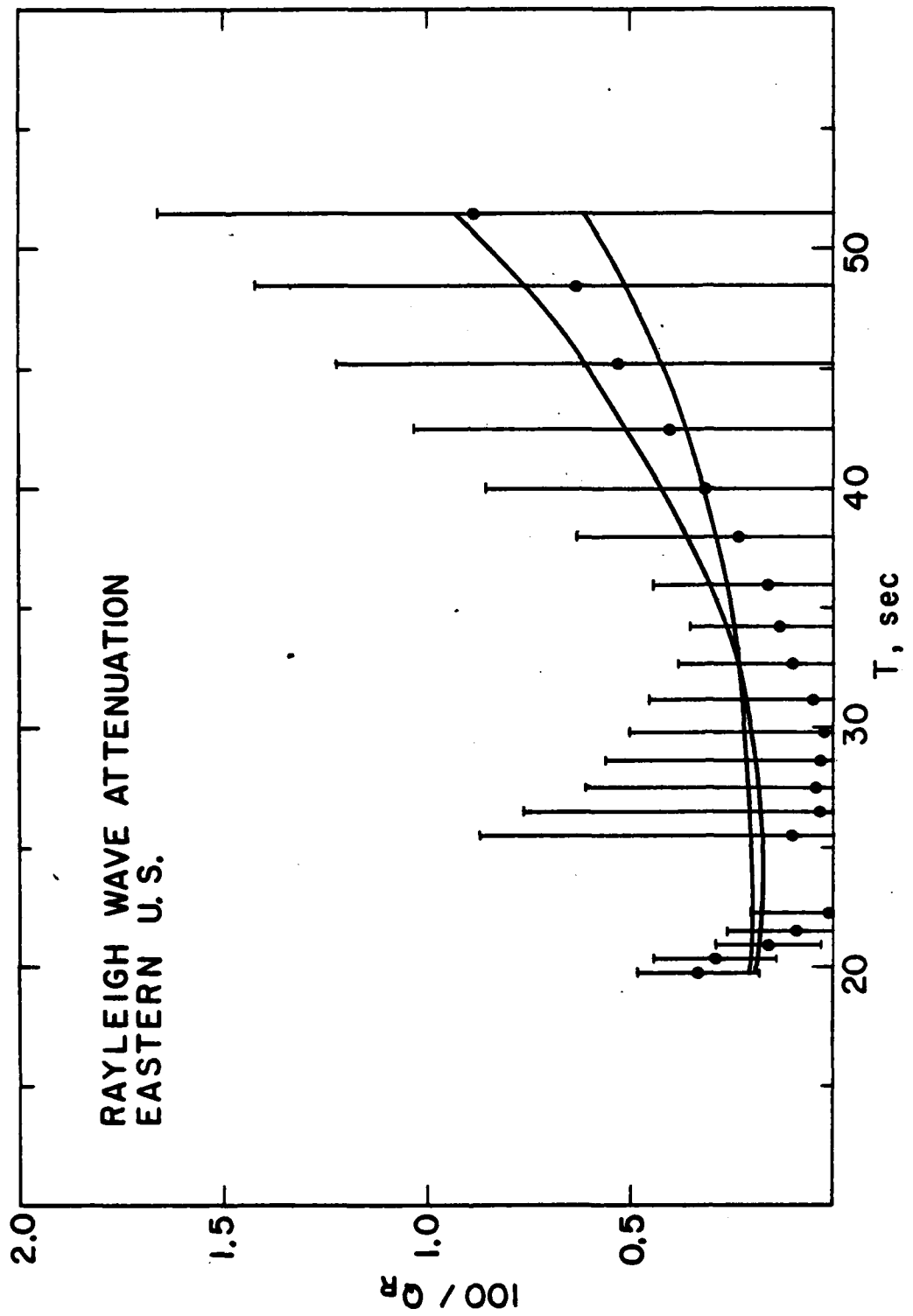
RAYLEIGH WAVE ATTENUATION
EASTERN U.S.
100 / Q_R
2.0
1.5
1.0
0.5
20
30
40
50
T, sec

Figure 15

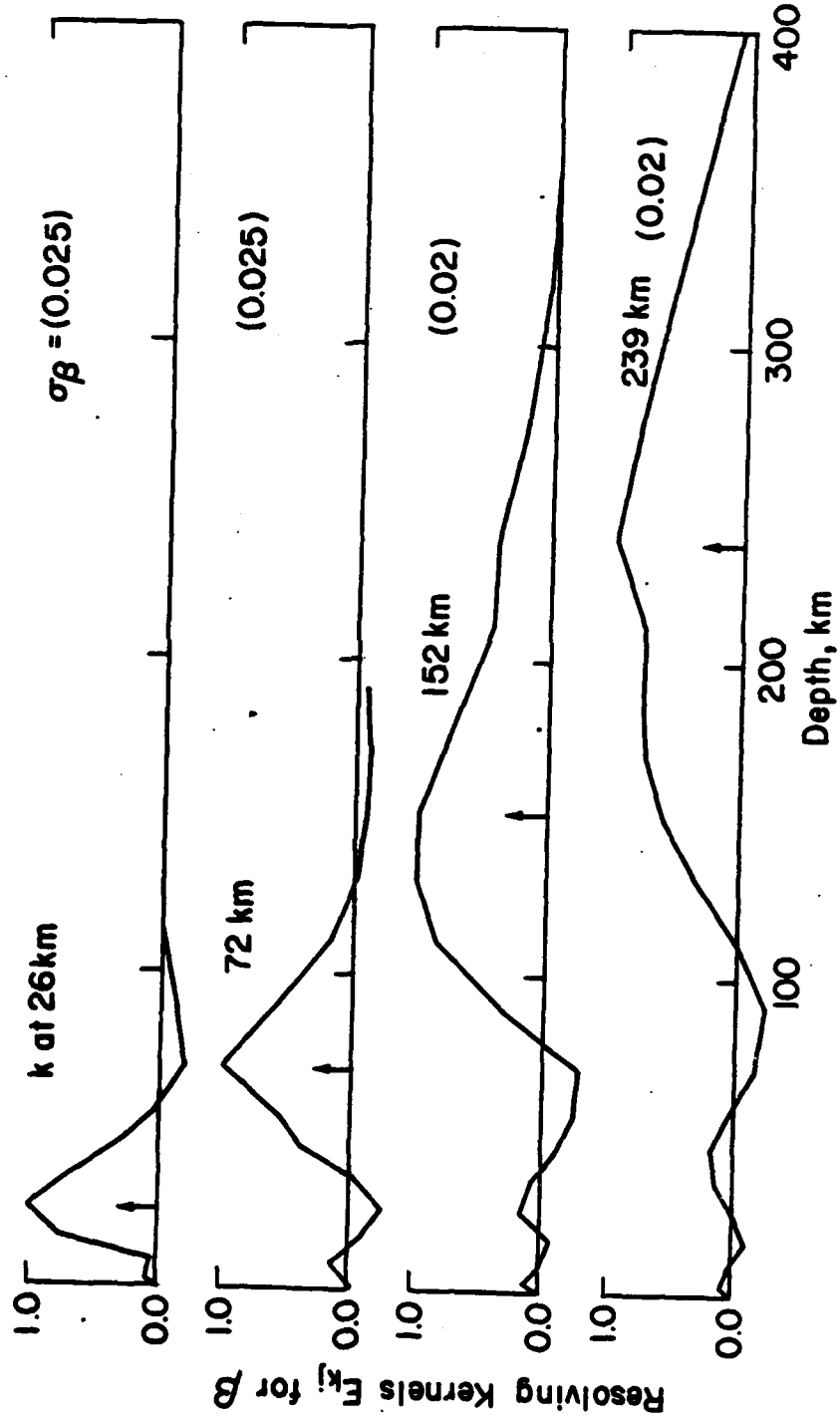
Resolving Kernels E_{kj} for β
1.0
0.0
k at 26km
$\sigma\beta$ =(0.025)
72 km
(0.025)
152 km
(0.02)
239 km
(0.02)
100
200
300
400
Depth, km

Figure 16a

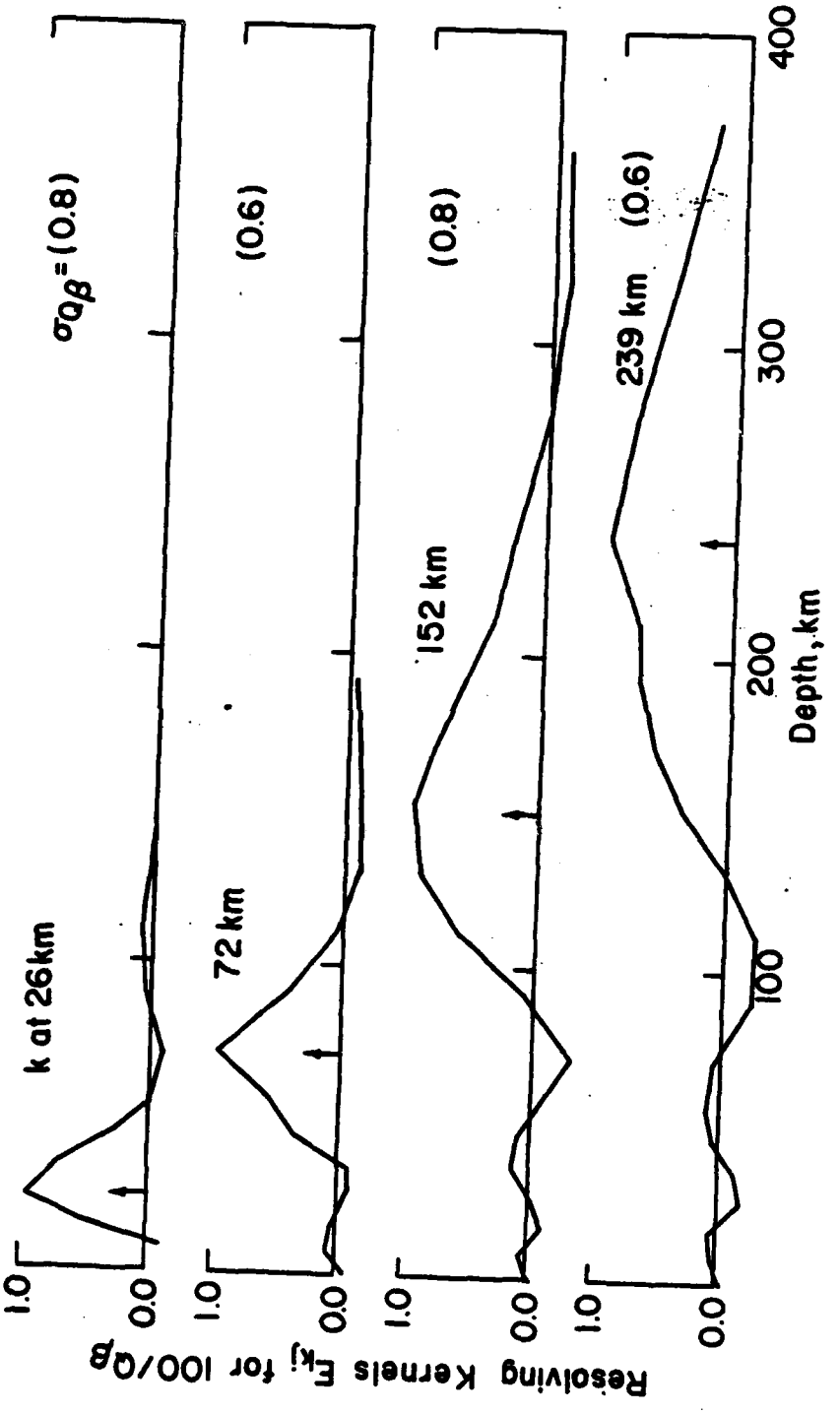
Resolving Kernels E_{kj} for $100/Q_\beta$
k at 26km
72 km
152 km
239 km
$\sigma_{Q\beta}$=(0.8)
(0.6)
(0.8)
(0.6)
1.0
0.0
100
200
300
400
Depth, km

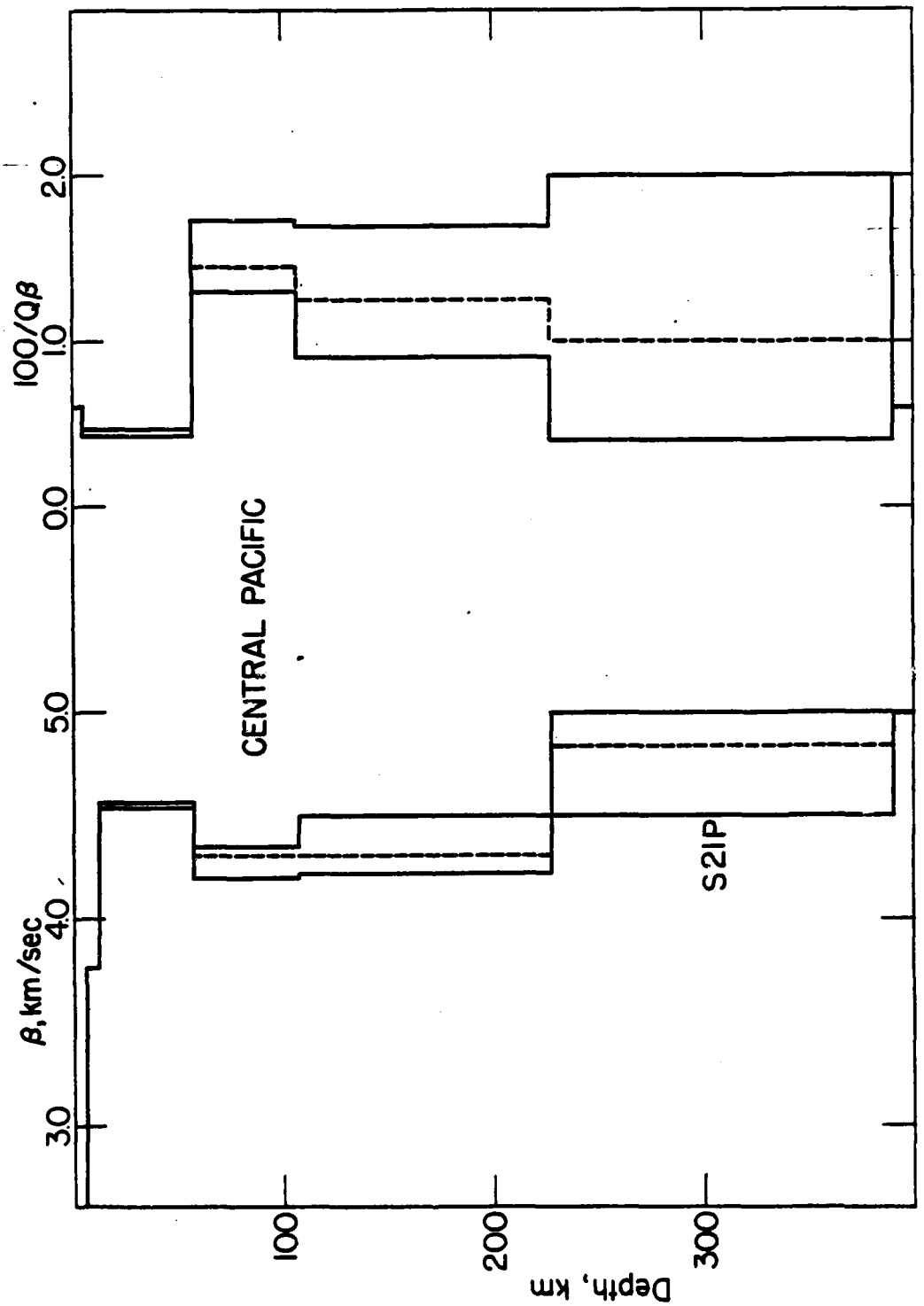
100/Qβ
2.0
1.0
0.0
5.0
CENTRAL PACIFIC
S21P
β, km/sec
4.0
3.0
100
200
300
Depth, km

Figure 17

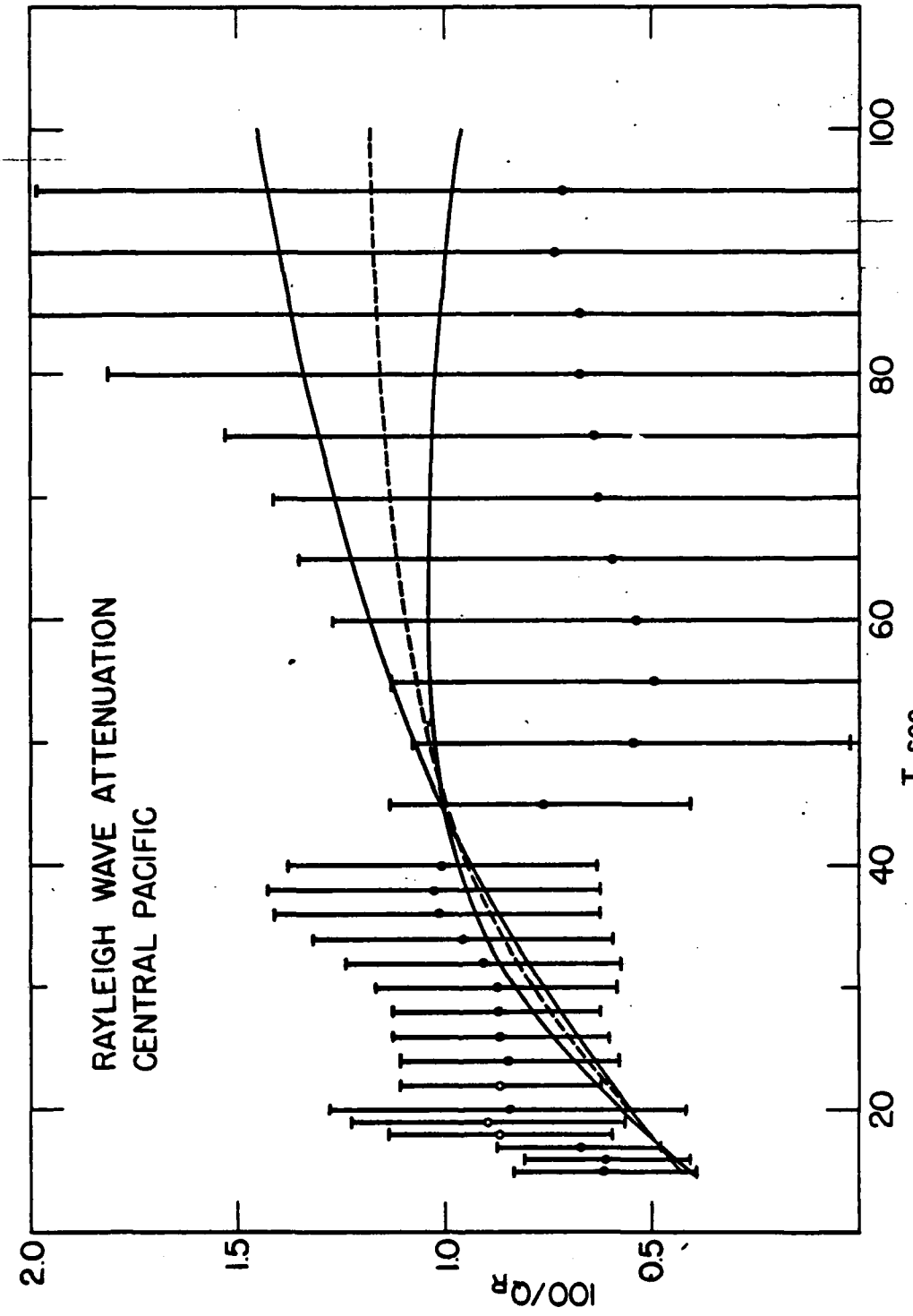
RAYLEIGH WAVE ATTENUATION
CENTRAL PACIFIC
100/Q_R
2.0
1.5
1.0
0.5
20
40
60
80
100
T, sec

Figure 18

4. CUMULATIVE LIST OF PUBLICATIONS UNDER THE PRESENT CONTRACT

Abe, K., Re-examination of the fault model for the Niigata earthquake of 1964, J. Phys. Earth, 23, 349-366, 1975.

Aki, K., A. Christoffersson and E. Husebye, Three-dimensional seismic structure of the lithosphere under Montana LASA, Bull. Seism. Soc. Am., 66, 501-524, 1976.

Aki, K., A. Christoffersson and E. Husebye, Determination of the three-dimensional seismic structure of the lithosphere, J. Geophys. Res., 82, 277-296, 1977.

Bird, P., Thermal and mechanical evolution of continental convergence zones, Ph.D. Thesis, M.I.T., Cambridge, Mass., 1976.

Bird, P. and M.N. Toksöz, Strong attenuation of Rayleigh waves in Tibet, Nature, 266, 161-163, 1977.

Bird, P., M.N. Toksöz and N.H. Sleep, Thermal and mechanical models of continent-continent convergence zones, J. Geophys. Res., 80, 4405-4416, 1975.

Burr, N.C., The relationship of source parameters of oceanic transform earthquakes to plate velocity and transform length, M.S. Thesis, M.I.T., Cambridge, Mass., 1977.

Burr, N. and S.C. Solomon, The relationship of source parameters of oceanic transform earthquakes to plate velocity and transform length, J. Geophys. Res., 83, 1193-1205, 1978.

Canitez, N., Optimum filter for surface-wave group velocity determination, Bull. Seism. Soc. Am., 67, 79-85, 1977.

Chapman, M.E. and S.C. Solomon, North American-Eurasian plate boundary in northeast Asia, J. Geophys. Res., 81, 921-930, 1976.

Husebye, E., A. Christoffersson, K. Aki and C. Powell, Preliminary results on the three-dimensional seismic structure of the lithosphere under the USGS central California seismic array, Geophys. J. R. Astr. Soc., 46, 319-340, 1976.

Johnston, D.H., The attenuation of seismic waves in dry and saturated rocks, Ph.D. Thesis, M.I.T., Cambridge, Mass., 1978.

Johnston, D.H., M.N. Toksöz and A. Timur, Attenuation of seismic waves in dry and saturated rocks, II. Mechanisms, Geophysics, in press, 1978.

Lee, W.B., Simultaneous inversion of surface wave phase velocity and attenuation for continental and oceanic paths, Ph.D. Thesis, M.I.T., Cambridge, Mass., 1977.

Lee, W.B. and S.C. Solomon, Inversion schemes for surface wave attenuation and Q in the crust and the mantle, Geophys. J. R. Astr. Soc., 43, 47-71, 1975.

Lee, W.B. and S.C. Solomon, Simultaneous inversion of surface wave phase velocity and attenuation: Love waves in western North America, J. Geophys. Res., 83, 3389-3400, 1978.

Lee, W.B. and S.C. Solomon, Simultaneous inversion of surface wave phase velocity and attenuation: Rayleigh and Love waves over continental and oceanic paths, Bull. Seism. Soc. Am., in press, 1978.

Madariaga, R., Dynamics of an expanding circular fault, Bull. Seism. Soc. Am., 66, 639-666, 1976.

Sengupta, M.K. and B.R. Julian, P-wave travel times for deep earthquakes, Bull. Seism. Soc. Am., 66, 1555-1579, 1976.

Sengupta, M.K. and M.N. Toksöz, Three dimensional model of seismic velocity variation in the earth's mantle, Geophys. Res. Lett., 3, 84-86, 1976.

Sengupta, M.K. and M.N. Toksöz, The amplitudes of P waves and magnitude corrections for deep focus earthquakes, J. Geophys. Res., 82, 2971-2980, 1977.

Solomon, S.C., Geophysical constraints on radial and lateral temperature variations in the upper mantle, Am. Mineral., 61, 788-803, 1976.

Solomon, S.C. and K.T. Paw U, Elevation of the olivine-spinel transition in subducted lithosphere: seismic evidence, Phys. Earth Planet. Int., 11, 97-108, 1975.

Toksöz, M.N., The subduction of the lithosphere, Sci. Amer., 233, 88-98, 1975.

Toksöz, M.N., E. Arpat and F. Saroglu, East Anatolian earthquake of 24 November 1976 - field observations, Nature, 270, 423-425, 1977.

Toksöz, M.N. and P. Bird, Formation and evolution of marginal basins and continental plateaus, in Island Arcs, Deep Sea Trenches and Back Arc Basins, eds. M. Talwani and W.C. Pitman III, Maurice Ewing Series, Vol. 1, 379-393, AGU, Washington, D.C., 1977.

Toksöz, M.N. and P. Bird, Modelling of temperatures in continental convergence zones, Tectonophysics, 41, 181-193, 1977.

Toksöz, M.N., J. Nabelek and E. Arpat, Source properties of the 1976 earthquake in E. Turkey: A comparison of field data and teleseismic results, Tectonophysics, 49, 199-205, 1978.

Ward, R.W. and K. Aki, Synthesis of teleseismic P waves from sources near sinking lithospheric slabs, Bull. Seism. Soc. Am., 65, 1667-1680, 1975.